

Electronic Thesis and Dissertation Repository

---

8-24-2017 10:00 AM

## Determining The Detective Quantum Efficiency (DQE) Of X-Ray Detectors In Clinical Environments

Terenz R. Escartin, *The University of Western Ontario*

Supervisor: Dr. Ian Cunningham, *The University of Western Ontario*

A thesis submitted in partial fulfillment of the requirements for the Master of Science degree in Medical Biophysics

© Terenz R. Escartin 2017

Follow this and additional works at: <https://ir.lib.uwo.ca/etd>



Part of the [Equipment and Supplies Commons](#), [Health and Medical Physics Commons](#), [Health Services Research Commons](#), and the [Investigative Techniques Commons](#)

---

### Recommended Citation

Escartin, Terenz R., "Determining The Detective Quantum Efficiency (DQE) Of X-Ray Detectors In Clinical Environments" (2017). *Electronic Thesis and Dissertation Repository*. 4819.  
<https://ir.lib.uwo.ca/etd/4819>

This Dissertation/Thesis is brought to you for free and open access by Scholarship@Western. It has been accepted for inclusion in Electronic Thesis and Dissertation Repository by an authorized administrator of Scholarship@Western. For more information, please contact [wlsadmin@uwo.ca](mailto:wlsadmin@uwo.ca).

## Abstract

According to Health Canada, dental and medical radiography accounts for more than 90% of total man-made radiation dose to the general population. Ensuring patients receive the health benefits of diagnostic x-ray imaging without use of higher radiation exposures requires knowledge and understanding of the detective quantum efficiency (DQE). Currently, the DQE is not measured in clinics because it requires specialized instrumentation and specific DQE-expertise to perform an accurate analysis. In this regard, the goals of this thesis were to: 1) address the limitations of measuring the DQE in clinical environments that affects the accuracy of the measurement; 2) develop and validate an automated method of measuring the DQE that is compliant with current regulatory standards to relieve experimental burden on the end-user. It is shown that the DQE can be measured with confidence using the automated method despite the limitations present in clinical environments. This work provides the opportunity for the clinical end-user who may not be familiar with the DQE-measurement process to accurately measure the DQE of clinical x-ray detectors, and provides the opportunity for the DQE to be a primary metric for quality assurance and control practices in the clinical environment.

### Keywords

detective quantum efficiency (DQE), x-ray image quality, x-ray detector performance, quality assurance

## Co-Authorship

Chapter 2 is being prepared for submission for publication in Radiology as the article analyzed “Detective Quantum Efficiency in the Clinical Setting” by Terenz Escartin, Tomi Nano and Ian A. Cunningham. I was responsible for experimental design, data acquisition, analysis and manuscript preparation under the supervision and confirmation of my supervisor, Dr. Ian Cunningham. Tomi Nano assisted with data acquisition, analysis and interpretation.

## Acknowledgements

First I would like to thank my supervisor Dr. Ian Cunningham for teaching me the fundamental concepts of Fourier theory that are necessary to appreciate and deeply understand x-ray imaging systems. I would also like to thank him for his encouragement on being a life-long learner by complimenting my extensive clinical background with the core mathematics and science that will help me excel in the field of medical imaging. To my advisory committee, Dr. Ting Yim Lee, Dr. Matthew Teeter, and Dr. George Hajdok, thank you for guidance and feedback. I would also like to thank Mr. Michael McDonald for his tireless work in providing the equipment I needed for experimentation in the lab. To Christiane Burton for her valued feedback in all the work I presented and performed in the lab. I would like to thank Mr. Alex Gontar and the Michener Institute for allowing us to use their digital detector systems for experimentation. To Patrick Caloracan and Jimmy Phan, thank you for making my move from Toronto to London a smooth experience with your occasional visits. Special thanks to Tomi Nano for all his help in brainstorming, modelling, and experimentation. My sincerest gratitude to Dr. Grace Parraga for guiding me towards joining a lab that consistently challenged me and pushed my limits. To Dante Capaldi, Eric Lessard, Rachel Eddy, Khadija Sheikh, Mark Henshaw, Olivia Stanley, Derek Gillies, Jessica Rodgers, Amy Schranz, Claire Vannelli, John Iyaniwura, Justin Michael, Fumin Guo, Dilraj Sanghera, and Tomi Nano, thank you for your friendship, support and for making my time at Western an enjoyable one. To my parents, thank you for your love and advice for planning towards a fulfilling and rewarding future.

# Contents

<b>Abstract</b>	<b>i</b>
<b>Co-Authorship Statement</b>	<b>ii</b>
<b>Acknowledgements</b>	<b>iii</b>
<b>Table of Contents</b>	<b>iv</b>
<b>List of Figures</b>	<b>vi</b>
<b>List of Symbols</b>	<b>xi</b>
<b>1 Introduction</b>	<b>1</b>
1.1 The Beginnings of X-Ray Imaging . . . . .	1
1.1.1 X-Ray Production . . . . .	2
1.1.2 Diagnostic X-Ray Imaging . . . . .	4
1.1.3 Screen-Film Radiography . . . . .	5
1.1.4 Limitations of Screen-Film Radiography . . . . .	8
1.1.5 Computed Radiography: How it works . . . . .	9
1.1.6 Transition to Computed Radiography . . . . .	9
1.1.7 Digital Radiography: Flat Panel Detectors . . . . .	11
1.1.8 Exposure Creep . . . . .	12
1.1.9 Patient Radiation Protection Initiatives . . . . .	14

1.1.10	Exposure Index . . . . .	14
1.2	Detective Quantum Efficiency (DQE) . . . . .	15
1.2.1	Linearization of Pixel Gain . . . . .	18
1.2.2	Modulation Transfer Function (MTF) . . . . .	19
1.2.3	Wiener Noise Power Spectrum . . . . .	20
1.3	Health Canada and Safety Code 35 . . . . .	22
1.4	Using DQE in X-ray Imaging . . . . .	23
1.5	DQE Measuring Device . . . . .	24
1.6	Research Objectives . . . . .	24
<b>2</b>	<b>Detective Quantum Efficiency (DQE) Measurements in a Clinical Setting</b>	<b>38</b>
2.1	Introduction . . . . .	39
2.2	Theory . . . . .	41
2.2.1	Air KERMA in Uncertain Image Plane . . . . .	42
2.2.2	MTF with Increased Edge-plate Distance . . . . .	43
2.2.3	Image Data Linearity . . . . .	45
2.2.4	Beam Half Value Layer . . . . .	46
2.3	Materials and Methods . . . . .	47
2.3.1	Detector Specifications . . . . .	47
2.3.2	Image Plane Air KERMA . . . . .	47
2.3.3	Determining the Focal Spot Profile . . . . .	48
2.3.4	Linearization . . . . .	49
2.3.5	Different Combinations of kV and Al Filtration . . . . .	50
2.4	Results . . . . .	52
2.4.1	Focal Spot Profile . . . . .	52
2.4.2	Image Plane Air KERMA Validation Using Fiducial Markers	53
2.4.3	Varying Distance of the MTF Edge from the Image Plane . . .	53

2.4.4	Varying Distance of the Beam Hardening Filter from the Focal Spot . . . . .	55
2.4.5	Different Combinations of kV and Al with the same HVL . . . . .	56
2.4.6	Linearized vs. Nonlinearized Image Data . . . . .	57
2.5	Discussion . . . . .	57
2.6	Conclusion . . . . .	59
2.7	Acknowledgements . . . . .	61
<b>3</b>	<b>Conclusions and Future Directions</b>	<b>67</b>
3.1	Overview and Research Questions . . . . .	68
3.2	Summary and Conclusions . . . . .	68
3.3	Limitations . . . . .	70
3.3.1	Manufacturer Specific Image Processing . . . . .	70
3.3.2	Extraction of Images . . . . .	71
3.3.3	Length of Time for Analysis . . . . .	71
3.4	Future Directions . . . . .	72
3.4.1	NEQ, DQE and the Exposure Index . . . . .	72
3.4.2	DQE and Technique Charts . . . . .	73
3.4.3	Cloud-Based Analysis of DQE . . . . .	74
3.4.4	DQE Survey of Digital Detectors . . . . .	74
3.5	Implications of Research . . . . .	75
<b>A</b>	<b>Copyright Permissions for Figures Used in Chapter 1</b>	<b>79</b>
	<b>Curriculum Vitae</b>	<b>83</b>

# List of Figures

1.1.1 Illustration of a Coolidge x-ray tube. . . . .	2
1.1.2 Schematic of the production of Bremsstrahlung radiation (left) and characteristic radiation (right). . . . .	3
1.1.3 Illustration of an x-ray spectrum with a that has a maximum energy of 76 kV. Spikes in the x-ray spectrum correspond with characteristic x-ray emission. . . . .	3
1.1.4 Illustration of diagnostic x-ray imaging set-up in a clinical environment.	4
1.1.5 Radiographic image of the hand (left). Mammography image of the breast (top middle). CT image of the thoracic area (bottom mid- dle). Barium swallow study under fluoroscopic image guidance (right). Case courtesy of Mr Andrew Murphy, Radiopaedia.org, rID: 48226. Case courtesy of A.Prof Frank Gaillard, Radiopaedia.org, rID: 12608. Case courtesy of Dr Andrew Dixon, Radiopaedia.org, rID: 36676. Case courtesy of Dr Ian Bickle, Radiopaedia.org, rID: 53859. . . . .	5
1.1.6 Characteristic response of an x-ray film (H&D cruve). . . . .	7
1.1.7 Illustration of an electron excited to a meta stable state by an incident x-ray photon (left). A laser restoring the excited electron back to its resting state to liberate visible light (right). . . . .	10
1.1.8 Illustration of indirect DR (left) and direct DR (right). Adapted from Sperrin M, X-ray Imaging (2014). <sup>75</sup> . . . . .	11



1.1.9	Illustration of radiographs taken from patients in the intensive care and critical care unit over 2 years. Adapted from Gibson DJ, Aca. Rad. (2012). <sup>32</sup> . . . . .	13
1.1.10	The top row illustrates simulated chest x-ray images that are underexposed (left), optimally exposed (middle), and overexposed (right) to describe a detector with a narrow exposure latitude. The bottom row illustrates simulated chest x-ray images that are underexposed (left), optimally exposed (middle), and overexposed (right) to the same degree as the top row to describe a detector with a wide exposure latitude. Over- and underexposed radiographs are more readily discernable when using detectors with a narrow exposure latitude. Case courtesy of Dr Usman Bashir, Radiopaedia.org, rID: 18394 . . . . .	13
1.1.11	Definition of exposure indices by different manufacturers. Adapted from Uffmann M et al, Eur. J. Radiol. (2009). <sup>78</sup> . . . . .	16
1.2.1	Illustration of the DQE of a digital detector . . . . .	18
1.2.2	Illustration of a detector with slightly non-linear characteristic response	19
1.2.3	The edge spread function ESF (top right) is determined from the slanted edge image (top left). The MTF (bottom right) is calculated by differentiating the ESF and taking the Fourier Transform of the LSF (bottom left) . . . . .	21
1.2.4	Illustration of the NPS in frequency space (left) and the one-dimensional normalized NPS (NNPS)(right) . . . . .	21
1.3.1	Illustration of the balance between image quality and exposure including the governing bodies that regulate exposure and the metrics currently used in clinics. . . . .	23
2.2.1	Illustration of focal-spot penumbral blur as the edge-image distance $d_e$ is increased. . . . .	43

2.2.2 Illustration of blur caused by scatter from the beam-hardening filter as the filter distance $d_f$ is increased. . . . .	44
2.2.3 Illustration of the characteristic curve from a detector with a very slight non-linear response causing the slope of the characteristic curve to vary with detector KERMA. The nominal exposure used to measure the DQE was $2.97 \mu\text{Gy}$ . System gain $G$ is equal to the local slope at the nominal exposure. . . . .	45
2.3.1 X-ray image of frame containing five fiducial markers on a $8.4 \times 8.4$ cm square. Pixel spacing at the frame position is given by the number of pixels between markers divided by physical distance. . . . .	48
2.3.2 Aluminum filtration and tube kV settings for a x-ray beam HVL of 6.8mm of Al. . . . .	51
2.3.3 a.) Comparison of simulated x-ray beams using different combinations of kV and Al to generate a 6.8 mm Al HVL b.) Comparison of simulated photon fluence absorbed in CsI from three x-ray beams. . . . .	52
2.4.1 a) System transfer function obtained using the slanted-edge method with the edge placed at 1.3 cm and 101.3 cm from the image plane. b) Focal spot intensity profile as determined with Eq. 2.2.4 . . . . .	52
2.4.2 Plot of image-plane KERMA determined using Eq. (2.2.1) as a function of chamber distance from the image plane (SID = 150 cm). Error bars represent uncertainties $\sigma_K$ determined by Eq. (2.2.2). The orange line shows the measured air KERMA using the ion chamber positioned at 150 cm . . . . .	53
2.4.3 a.) MTF plot at different distances using a 150 cm SID, b.) MTF plot at different distances using a 100 cm SID . . . . .	54

2.4.4 a.) MTF plot with the edge placed 13 mm from the image plane using a 150 cm SID while changing the SFD, b.) MTF plot with the edge placed at 103 mm from the image plane using a 150 cm SID. . . . .	55
2.4.5 c.) MTF plot with edge placed at 13 mm from the image plane using a 100 cm SID, and d.) MTF plot with edge placed at 103 mm from the image plane using a 100 cm SID. . . . .	56
2.4.6 a.) Comparison of DQE curves acquired with different x-ray beams having the same HVL=6.8mm of Al but different kV and filtration. These DQEs were measured on the same detector with the same nominal air KERMA. b.) Ratio of DQE of the four spectra relative to the standard RQA-5 spectrum. . . . .	56
2.4.7 Comparison of DQE results using linearized vs. non-linearized image data. . . . .	57
3.4.1 Illustration of DQE as a potential standardized metric used in combination with NEQ and EI to quantitatively sustain the balance between image quality and exposure . . . . .	73

## List of Symbols

<b>Symbol</b>	<b>Definition</b>
2D	Two-dimensional
kV	kilovoltage
mA	milliamperes
mAs	Current-time product (milliampere-seconds)
CT	Computed Tomography
ALARA	As Low As Reasonably Achievable
SF	Screen-Film
OD	Optical Density
H&D	Hurter-Driffield
CR	Computed Radiography
DMIST	Digital Mammographic Imaging Screening Trials
DR	Digital Radiography
RSNA	Radiological Society of North America
AAPM	American Association of Physicists in Medicine
ESPR	European Society of Paediatric Radiology
AOSPR	Asian-Oceanic Society for Paediatric Radiology
EI	Exposure Index
IEC	International Electrotechnical Commission
KERMA	Kinetic Energy Released Per Unit Mass
DI	Deviation Index
MTF	Modulation Transfer Function
NPS	Noise Power Spectrum
NEQ	Noise Equivalent Quanta

DQE	Detective Quantum Efficiency
SC35	Safety Code 35
CAMRT	Canadian Association of Medical Radiation Technologists
HARP	Healing Arts and Radiation Protection Act
SNR	Signal-to-Noise Ratio
FDA	Food and Drug Administration
CID	Chamber-to-Image Distance
SID	Source-to-Image Distance
Al	Aluminum
HVL	Half Value Layer
CsI	Cesium Iodide
$I_t$	Trasmitted fraction of light
$I_0$	Incident number of light quanta
$K_{IND}$	Air KERMA incident on the digital detector
$K_{TGT}$	Target equivalent air KERMA
$\bar{q}$	Average number of incident quanta
G	Detector gain
LSF(x)	Line Spread Function
ESF(x)	Edge Spread Function
OTF(u)	Optical Transfer Function
W(u)	Wiener Noise Power Spectrum
NNPS(u)	Normalized Noise Power Spectrum
$K_f$	Autocovariance function
$\bar{d}$	Average digital value
$Q_0$	Number of x-ray quanta per unit area per unit KERMA
T(u)	Transfer Function

$K$	Image plane air KERMA
$K_c$	Chamber plane air KERMA
$d_s$	Source Image Plane Distance
$d_c$	Chamber Image Plane Distance
$a_c$	Pixel spacing at chamber plane
$a$	Pixel spacing at image plane
$\sigma_K^2$	Variance in image plane air KERMA
$\sigma_{K_c}^2$	Variance in chamber plane air KERMA
$\sigma_{a_c}^2$	Variance in pixel spacing at chamber plane
$f(x')$	Focal spot profile
$x'$	Position on the x-ray source
$f(x)$	Penumbral blur on image
$x$	Position in the image plane
$d_e$	Edge-image distance
$T_f(u)$	Focal spot transfer function
$F(u)$	Fourier Transform of penumbral blur on image
$T_s(u)$	Filter scatter transfer function
$DQE_{\Delta}(u)$	DQE of non-linear system
$\alpha$	Quantum efficiency
$E$	X-ray Energy
$\mu$	Mass attenuation coefficient
$\rho$	Material density
$l$	Converter material thickness

# Chapter 1

## Introduction

### 1.1 The Beginnings of X-Ray Imaging

X-rays were first discovered in 1895 by Wilhelm Roentgen. In 1896, he published his discovery and showed it was possible to obtain a radiographic image of a human hand.<sup>60</sup> Before 1912, x-rays were seldom used in medical applications because x-ray tubes malfunctioned when using high voltages to produce x-rays with sufficient penetrating power to acquire a radiograph. This limitation was resolved in 1913 when the Coolidge tube was developed by William Coolidge that allowed for use of x-rays more readily in clinical settings (Fig. 1.1.1).<sup>16</sup> Use of x-rays for medical imaging purposes exposes the patient to radiation to acquire a diagnostic image. According to Health Canada, dental and medical radiography is the largest contributor of man-made radiation exposure to the population, accounting for more than 90% of total man-made radiation dose to the general population. In 2007, it was estimated that two-dimensional (2D) x-ray imaging constitutes 65% of all medical imaging procedures performed in Canada<sup>36</sup>. X-ray imaging has established its role as the primary medium for evaluating and confirming patient condition for most diagnostic imaging procedures, ranging from urgent trauma cases to longitudinal screening for breast

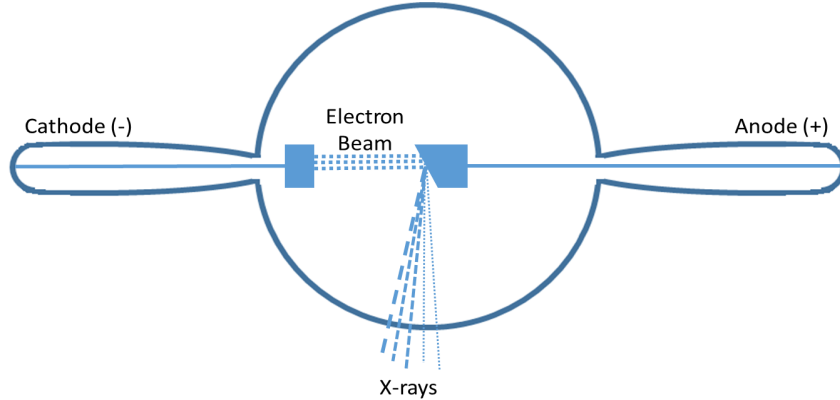


Figure 1.1.1: Illustration of a Coolidge x-ray tube.

### 1.1.1 X-Ray Production

X-ray production requires an x-ray tube made up of a negatively charged cathode and a positively charged anode. The cathode filament and target anode are typically made of a tungsten or molybdenum alloy because of their inherent capacity to tolerate high temperatures.<sup>76</sup> This is necessary because the cathode filament is heated substantially to generate and emit a high-energy electron beam towards the anode. The acceleration of the electron beam is primarily due to thermionic emission and the high potential difference between the cathode and anode. Bending and deceleration of the electron beam because of the positively charged nucleus of a tungsten or molybdenum atom in the target anode generates the x-ray beam. As the electron beam decelerates and bends towards the nucleus, it continuously loses some of its kinetic energy that is subsequently converted to a continuum of x-rays of different energies known as Bremsstrahlung radiation (Fig. 1.1.2). Bremsstrahlung or “braking radiation” is the primary process for x-ray production that makes up the majority of the x-ray spectrum. X-ray photons that make up the lesser portion of the x-ray spectrum are known as characteristic radiation (Fig. 1.1.2).



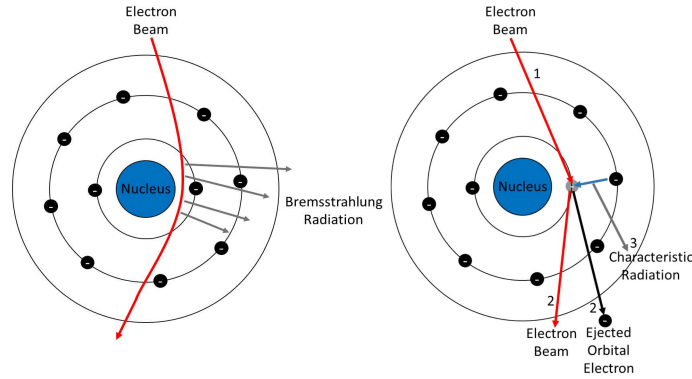


Figure 1.1.2: Schematic of the production of Bremsstrahlung radiation (left) and characteristic radiation (right).

Characteristic radiation emissions are the result of an ionization process that occurs when the incident electron beam expels an inner shell electron having a binding energy equivalent to or less than the energy of the incident electron beam. The components that control the shape of the x-ray spectrum include: 1) kilovoltage (kV); 2) milliamperes (mA); and 3) time (s). The kV is the x-ray tube potential that accelerates the electron beam from the cathode to the target anode that determines the penetrability of the x-ray beam. The mA is related to the current used to generate the electron beam that determines the number of x-ray photons in the x-ray beam. The x-ray spectrum can be described by identifying the number of x-ray photons per unit area as a function of x-ray photon energy (Fig. 1.1.3). These parameters that dictate the resulting x-ray spectrum are used to control the x-ray exposures used on patients to generate a radiographic image.

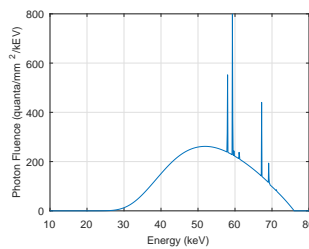


Figure 1.1.3: Illustration of an x-ray spectrum with a that has a maximum energy of 76 kV. Spikes in the x-ray spectrum correspond with characteristic x-ray emission.

## 1.1.2 Diagnostic X-Ray Imaging

Clinical applications of x-rays for diagnostic purposes are known as diagnostic x-ray imaging. It involves positioning a patient in between the x-ray tube and the detector to acquire a radiographic image of the anatomy of interest (Fig 1.1.4).

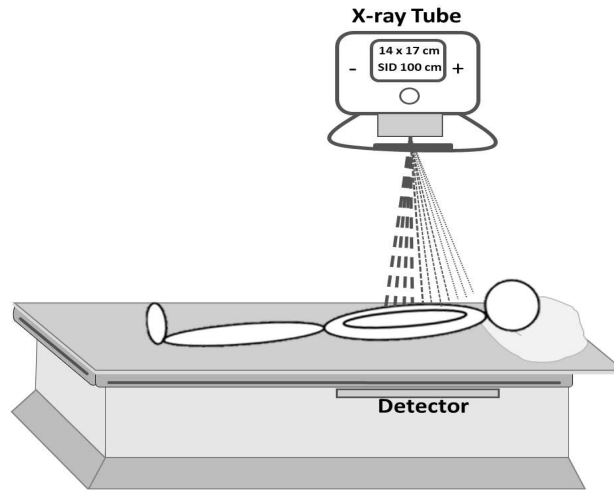


Figure 1.1.4: Illustration of diagnostic x-ray imaging set-up in a clinical environment.

Diagnostic x-ray images of a patient are typically performed to evaluate underlying pathological conditions that are not readily discernible through immediate physical examination, or to confirm an initial differential diagnosis. There are a number of diagnostic x-ray imaging modalities used in the clinical environment that include: 1) two-dimensional (2D) radiography; 2) two-dimensional (2D) mammography; 3) fluoroscopy; and 4) computed tomography (CT). Each modality provides different information about patient anatomy and physiology that adds to the physician's comprehensive list of medical information for diagnosis. Radiography provides immediate anatomical information about bone and soft tissue features (Fig 1.1.5). Mammograms provide high resolution images of breast tissue (Fig. 1.1.5). Fluoroscopy allows for real-time x-ray imaging for functional and physiological studies (Fig. 1.1.5). CT provides 3D reconstructions of structural anatomy that can be used concomitantly with contrast agents for functional and physiological evaluation (Fig. 1.1.5). The prescrip-

tion of an x-ray exam is based on clinical evaluation of the patient with the purpose of obtaining diagnostic information.<sup>12</sup> However, exposure to x-rays in clinical imaging poses a small risk to the patient in developing new cancers.<sup>46;37;6</sup> Therefore, the need for an x-ray exam must always be justified by ensuring the benefits always outweighs the risks associated with the procedure. In medical x-ray imaging, this is called the as low as reasonably achievable (ALARA) principle. It is considered to be an integral part of delivering standard patient care.

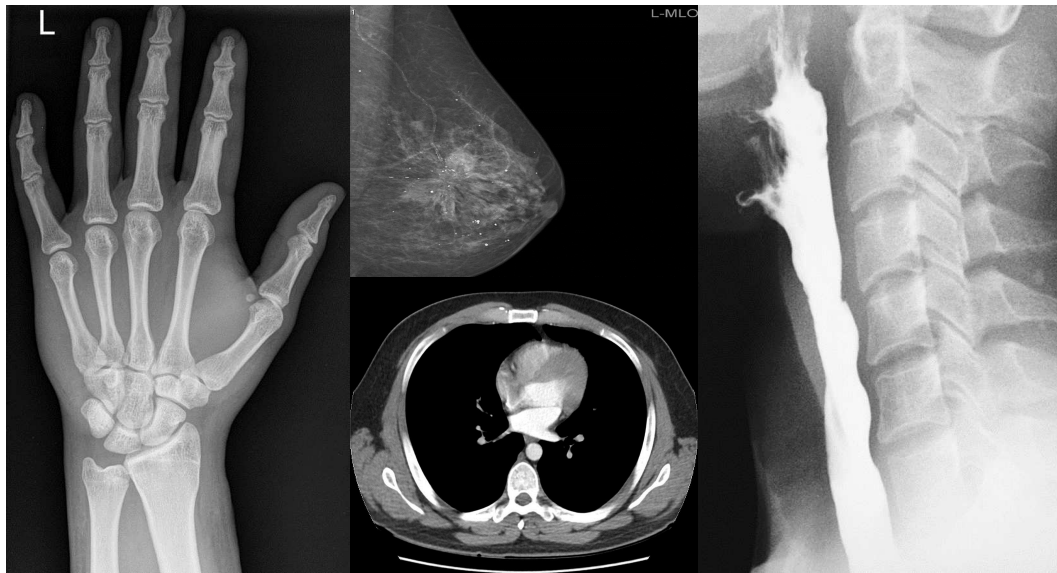


Figure 1.1.5: Radiographic image of the hand (left). Mammography image of the breast (top middle). CT image of the thoracic area (bottom middle). Barium swallow study under fluoroscopic image guidance (right). Case courtesy of Mr Andrew Murphy, Radiopaedia.org, rID: 48226. Case courtesy of A.Prof Frank Gaillard, Radiopaedia.org, rID: 12608. Case courtesy of Dr Andrew Dixon, Radiopaedia.org, rID: 36676. Case courtesy of Dr Ian Bickle, Radiopaedia.org, rID: 53859.

### 1.1.3 Screen-Film Radiography

One of the earlier types of clinical x-ray detectors used to generate a radiographic image used a x-ray screen and film (SF). X-ray films were coupled with an intensifying screen that had a higher absorption efficiency for x-ray photons than the x-ray film itself in order to reduce the number of incident x-rays needed to form an x-ray

image. This is particularly important in diagnostic x-ray imaging because it means the exposure used to acquire a radiographic image of the patient can be reduced. The x-ray photons incident to the intensifying screen are converted to light, and subsequently interact with the x-ray film to generate an invisible or latent image. The x-ray film containing the latent image is subsequently fed to a processor that houses various chemical agents to develop exposed silver halide crystals in order to render the radiographic image. The radiographic image is composed of different gray shades. Darker regions correspond with silver halide crystals being exposed to higher flux and energy light photons from the intensifying screen. Therefore, the entire radiographic image is a gradient of differing levels of darkness or brightness that can be described in terms of optical density. Optical density is a logarithmic function that is defined as:

$$\text{OD} = \log_{10} \frac{I_t}{I_0} \quad (1.1.1)$$

where  $I_t$  is the proportion of transmitted light through an exposed and developed x-ray film relative to the incident number of light quanta  $I_0$ . Darker regions in an x-ray film image that correspond with higher exposed crystals will absorb more light when viewed under fluorescent light. The optical density as a function of log exposure gives the characteristic response of the x-ray film also known as the Hurter-Driffield (H&D) curve (Fig. 1.1.6).

The toe of the curve represents exposures that would result in underexposed images, while the shoulder of the curve would result in overexposed images. Any x-ray image acquired using exposures that correspond with the shoulder or toe of the H&D curve hold no diagnostic value because of poor image quality owing to poor image contrast. Poor image quality hinders the ability to identify and diagnose pathologies

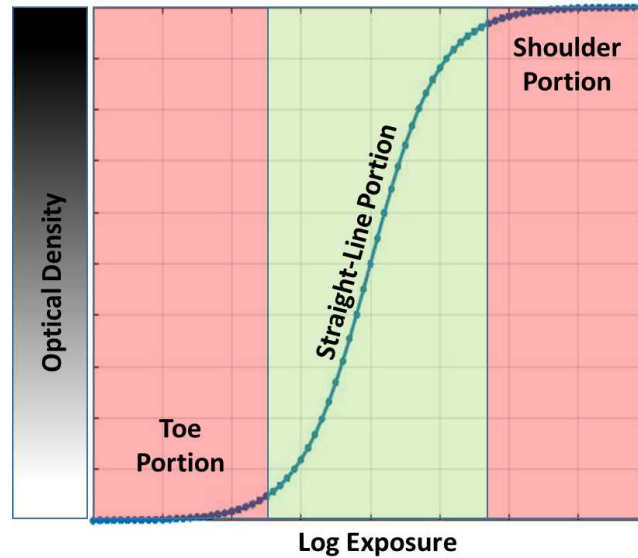


Figure 1.1.6: Characteristic response of an x-ray film (H&D curve).

concerning the patient, therefore additional x-ray images will need to be taken resulting in increased patient exposures. The straight-line portion of the H&D curve characterizes the exposure latitude of an x-ray film. It describes the x-ray exposures required for a specific x-ray film that will provide diagnostic quality x-ray images with sufficient image contrast. Therefore, x-ray images must be acquired within the exposure latitude of a given film in order to prevent acquiring low quality images and increasing patient exposures.

Since over- and underexposure of the x-ray film was readily identified by qualitatively evaluating image contrast, SF imaging was a self-regulating method from a patient radiation protection standpoint. X-ray technologists became highly skilled at selecting exposures to acquire high quality diagnostic images that kept patient exposures as low as reasonably achievable (ALARA). This is particularly important because there is always an added risk in developing new cancers when using ionizing x-rays as a diagnostic imaging tool. So, why move towards digital x-ray imaging?

#### 1.1.4 Limitations of Screen-Film Radiography

In the 1990s, use of SF systems in mammography was shown to be effective in breast cancer screening when used alongside physical breast examination.<sup>9;57;51;29</sup> However, managing an imaging facility that uses SF methods incurred economically unfavorable costs that include dedicated film storage, purchase of non-reusable x-ray films, film processing chemicals to develop the x-ray image, and the inefficient delivery of confidential patient health information in large facilities.<sup>77;62;9</sup> One of the biggest limitations of SF systems was a limited dynamic range. For SF systems, dynamic range is the ratio of the exposure corresponding with the maximum optical density that is related to the shoulder portion of the H&D curve to the exposure corresponding with the minimum optical density that is related to the toe portion of the H&D curve. Limited dynamic range affects the ability to discern and differentiate normal vs. abnormal breast tissue that is important for early cancer detection.<sup>13;39;40;62</sup> Furthermore, SF imaging did not allow for optimization of individual imaging components composed of the detector, display device and picture archiving communications systems that could aid in improving the contrast in the images. It soon became clear that further improvements in detector technology were needed to improve delineation of fine resolution differences between normal and abnormal breast tissue. In September 1991, the National Cancer Institute arranged a meeting between groups of breast imaging experts to discuss the most beneficial allocation of future research dollars to address conventional mammography limitations.<sup>56;74</sup> It was concluded that large investments should be made towards the development of digital mammography. This perhaps contributed to the paradigm shift among the scientific and medical imaging community to improve diagnostic x-ray imaging technology altogether.

### **1.1.5 Computed Radiography: How it works**

Computed Radiography (CR) was the initial method for generating digital x-ray images. It acquires a x-ray image digitally by using phosphor plates that interact with an incident number of x-ray quanta. This results in the excitation of electrons within the phosphor layer (Fig. 1.1.7). The electrons remain in an excited state until the plate is processed using a digitizer containing a laser that scans through the entire plate to bring the excited electrons back to resting state (Fig. 1.1.7). The energy liberated by the electron when returning to its resting state in the form of optical light is mapped to generate a digital x-ray image that is ultimately displayed on a monitor screen. The digital format when using CR plates for x-ray imaging opened new avenues for bettering diagnostic x-ray imaging. It provided a way to post-process the x-ray images as an additional aid to improve image readability. Digitization of the CR plate also allows for use of a wider range of exposures relative to film without sacrificing the diagnostic quality of the image. Earlier investigations regarding exposure reduction to patients when using CR relative to SF revealed much controversy, with some studies suggesting the performance of CR was either comparable to film or showed minimal effects or close to no effects in improvement of cancer detection and reducing patients exposures.<sup>85;70;47;65;41</sup> With progress being made in CR technology,<sup>43;17</sup> the imaging community continued to improve detector technology to reduce patient exposures.

### **1.1.6 Transition to Computed Radiography**

The transition between SF to CR did not follow a smooth path. In 1996, the FDA published the “Information for Manufacturers Seeking Marketing Clearance of Digital Mammography Systems” document outlining the requirements needed to acquire a pre-market approval (PMA) or 510(k) clearance that expedites the regulatory process of moving new digital mammography systems to clinical trials and the market.<sup>56</sup> To acquire a PMA or 510(k) clearance, manufacturers must show that the interpretations

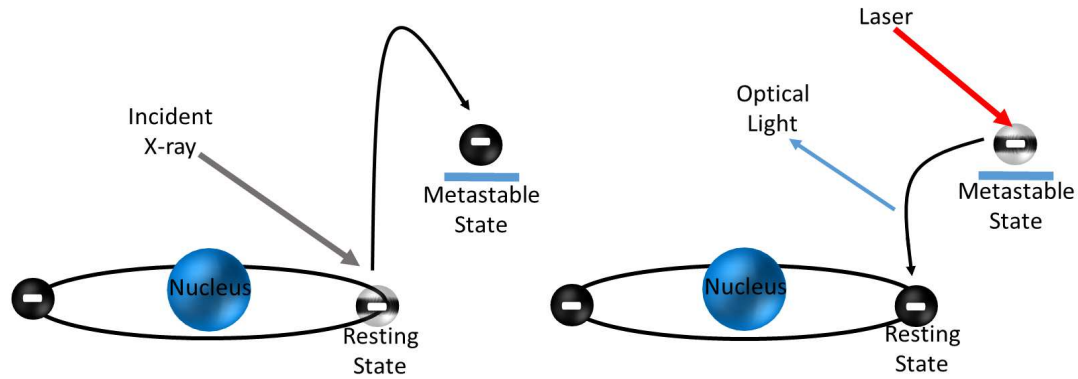


Figure 1.1.7: Illustration of an electron excited to a meta stable state by an incident x-ray photon (left). A laser restoring the excited electron back to its resting state to liberate visible light (right).

of x-ray images acquired using their digital systems agreed with existing SF images. Unfortunately, this initial guideline was found to be flawed and unreasonable due to issues with inter- and intrareader variability, differences in breast positioning, and breast compression that made it almost impossible for manufacturers to satisfy. Following the amendment of this document, the Digital Mammographic Imaging Screening Trials (DMIST) conducted clinical trials to compare the diagnostic accuracy of SF with CR for breast cancers. The study enrolled over 40,000 patients in the US and Canada who underwent breast imaging using both SF and CR. The results from the study was reported in 2005 suggesting that the diagnostic accuracy of CR and SF mammography were similar. However, the accuracy of CR was significantly higher than film among women under the age of 50, with women with heterogeneously dense or extremely dense breasts, and premenopausal or perimenopausal women<sup>55</sup>. Knowing that the diagnostic accuracy of CR and SF are comparable gave confidence to both the scientific and clinical imaging community to invest crucial time and dollars to to further improve digital x-ray imaging.<sup>49;4</sup> Advances in detector designs also contributed to the birth of a new era in digital radiography with the development of flat panel detectors that no longer required the intermediate step of processing a phosphor plate before seeing the digital image.<sup>44</sup>



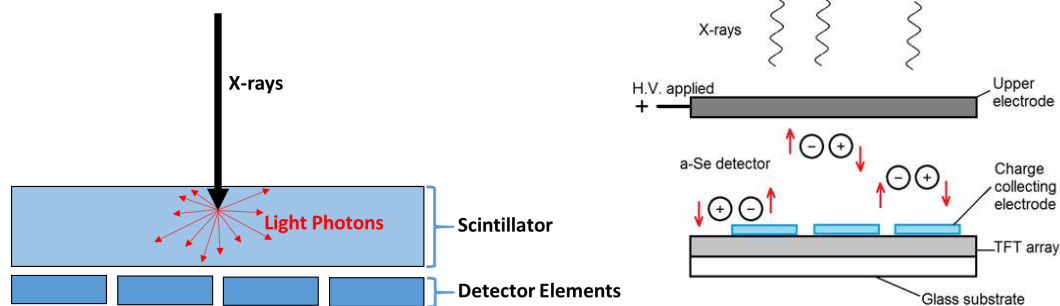


Figure 1.1.8: Illustration of indirect DR (left) and direct DR (right). Adapted from Sperrin M, X-ray Imaging (2014).<sup>75</sup>

### 1.1.7 Digital Radiography: Flat Panel Detectors

The two types of flat panel digital radiography (DR) detectors follow an indirect and direct conversion of x-ray photon energy to electronic signal. Indirect DR detectors make use of a scintillator to convert incident x-ray photons to light, which are subsequently converted to an electronic signal (Fig. 1.1.8). Direct DR detectors make use of a photo-conductor material that absorbs the incident x-ray photons to ionize atoms in the photoconductor layer generating electron-hole pairs (Fig. 1.1.8). The migration of charges to opposite ends of the photoconductor layer leads to immediate conversion of x-ray photon energy to electronic signal. Unlike CR, DR technology allows for almost instantaneous image acquisition and display while retaining the advantages of acquiring diagnostic x-ray images over a broad exposure range.

Investigators have suggested the coexistence of both CR and DR detectors due to improvements in CR technology.<sup>17;69</sup> However, advantages offered by DR extends beyond the convenience of instantaneous image acquisition and display. Reports have suggested that DR is superior to both CR and SF for dose reduction while maintaining high image quality.<sup>38;77;5;62;87;52;54</sup> Despite the potential for reducing patient exposures in CR and DR, a slight drift in increased patient exposures over time, also known as exposure creep, was observed upon adoption of either technology. This is owed to the fact that brightness and contrast of x-ray images acquired using CR and DR

detectors are less readily recognizable. This is made possible by the inherently wider exposure latitude offered by CR and DR detectors relative to SF detectors that make them more tolerable to over- and underexposures. Therefore, there is an increased risk in patients receiving higher exposures for every x-ray imaging procedure.

### 1.1.8 Exposure Creep

Radiation exposure to patients is often determined by use of technique charts that specify the optimal kV and mAs settings for a given x-ray procedure. While these technique charts serve as a guide to the technologist, they may be set differently between system to system. Therefore, exposures used for a given x-ray procedure can vary depending on the technologist and the x-ray system used. Erring on the side of higher exposure techniques can compensate for low performing systems. The gradual increase of exposure used over time is known as exposure creep. Exposure creep happens because over- and underexposure to the patient can no longer be readily distinguished qualitatively by evaluating the brightness and contrast of the x-ray image (Fig. 1.1.10). Many studies have raised this issue in order to bring awareness to all healthcare professionals of its existence for proactive actions to take place.<sup>47;78;23;25;46</sup> Exposure creep has been reported to be most acute in portable examinations, where x-ray procedural set-up is set manually by the technologist.<sup>85;78</sup> A study showed a 20% increase in over exposures in the intensive and critical care unit for chest x-ray imaging procedures over the course of 2 years (Fig. 1.1.9).<sup>32</sup> As a result, the patient is left vulnerable to being exposed to high radiation. The medical imaging community has addressed the significance of exposure creep by informing professionals involved with maintenance and use of x-ray imaging systems on how to mitigate and minimize the incidence of exposure creep.<sup>24;25;15;46</sup>

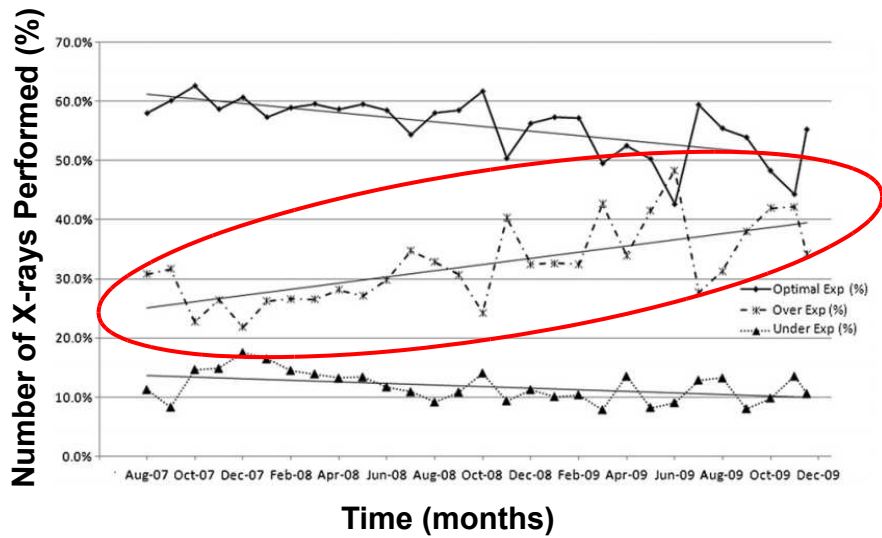


Figure 1.1.9: Illustration of radiographs taken from patients in the intensive care and critical care unit over 2 years. Adapted from Gibson DJ, Aca. Rad. (2012).<sup>32</sup>

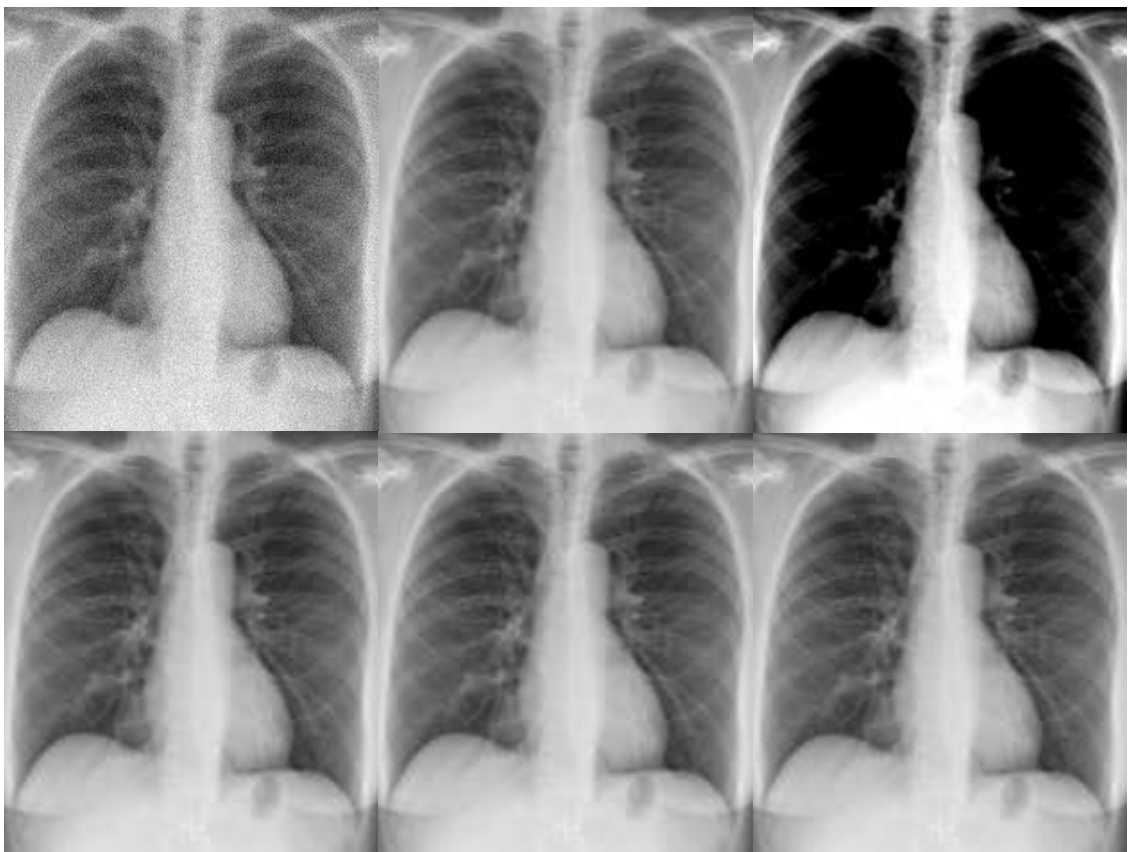


Figure 1.1.10: The top row illustrates simulated chest x-ray images that are underexposed (left), optimally exposed (middle), and overexposed (right) to describe a detector with a narrow exposure latitude. The bottom row illustrates simulated chest x-ray images that are underexposed (left), optimally exposed (middle), and overexposed (right) to the same degree as the top row to describe a detector with a wide exposure latitude. Over- and underexposed radiographs are more readily discernable when using detectors with a narrow exposure latitude. Case courtesy of Dr Usman Bashir, Radiopaedia.org, rID: 18394

### 1.1.9 Patient Radiation Protection Initiatives

Radiation protection initiatives have been formed to improve and identify issues regarding current standard of care practices to ensure safe and effective clinical x-ray imaging. Initiatives like the Image Gently alliance was first formed in late 2006 to safeguard pediatric patients from unnecessary exposure to radiation due to x-ray imaging, and raise awareness in the imaging community to optimize pediatric imaging.<sup>50;35;24;23;34;33</sup> The Image Wisely campaign was formed with the objective of lowering exposures used in medical imaging studies for the adult population.<sup>8;7;61;86</sup> Efforts from both alliances are supported by many reputable medical imaging organizations around the world like, the Radiological Society of North America (RSNA), American Association of Physicists in Medicine (AAPM), European Society of Paediatric Radiology (ESPR), and Asian-Oceanic Society for Paediatric Radiology (AOSPR). These organizations are involved in improvement of imaging technology and their use in clinics. They also address current issues regarding effective use of radiation for the purposes of medical imaging, and act on how to minimize exposures. For example, the AAPM Task Group 116 has reported and recommended use of the exposure index as a helpful marker for estimating radiation exposures used on patients for specific x-ray imaging procedures.<sup>73</sup>

### 1.1.10 Exposure Index

The exposure index (EI) provides information to the user whether sufficient exposure has reached the detector, thereby suggesting a diagnostic quality x-ray image has been acquired. The International Electrotechnical Commission (IEC) 62494-1 document provides specific definitions and requirements for the EI of images acquired using digital radiographic systems for CR and flat panel DR systems. The AAPM Task Group 116 made recommendations for all digital detectors to provide an indicator for the x-ray beam air KERMA (kinetic energy released per unit mass)  $K_{IND}$  incident

on the digital detector used to create the radiographic image.<sup>73</sup> This measurement indicates the quantity of radiation that was incident on the detector for each exposure. It is compared to a target equivalent air KERMA  $K_{TGT}$  that should result from any image when the detector is properly exposed.  $K_{TGT}$  is established by the user and/or manufacturer that is stored as a table in the system. The  $K_{IND}$  is used to compare with  $K_{TGT}$  in the form of a deviation index (DI) to determine whether each exposure was optimal. The DI is defined as:<sup>73</sup>

$$DI = 10 \log_{10} \frac{K_{IND}}{K_{TGT}}. \quad (1.1.2)$$

Since  $K_{IND}$  is dependent on the for-processing pixel values of each detector system and  $K_{TGT}$  is set uniquely by each manufacturer, users are left with multiple metrics that are defined differently to determine whether or not optimal exposures are being used for each procedure (Fig. 1.1.11). Furthermore, some studies have come to question whether manufacturers settings for EIs are too high, and the reliability of using the EI as a feedback mechanism for patient exposures.<sup>53;80;11</sup> Vast variabilities in the definition of EI compounded with access to detectors with wider exposure latitude heightens the likelihood for exposure creep across different clinical settings. This leaves much room for the acquisition of over- and underexposed images that ultimately results in increased patient radiation exposures.

## 1.2 Detective Quantum Efficiency (DQE)

The detective quantum efficiency (DQE) quantitatively describes the dose efficiency of x-ray detectors. It is described as the effective fraction of x-ray quanta contributing to image signal-to-noise (SNR) as a function of spatial frequency while considering additional image noise introduced by the detector.<sup>71</sup> It is a surrogate measure of the

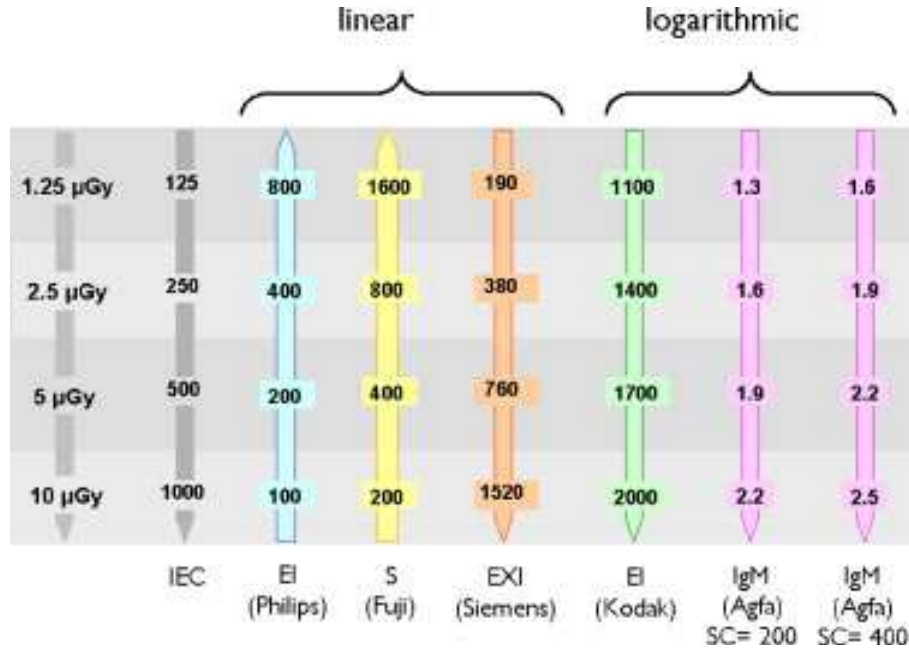


Figure 1.1.11: Definition of exposure indices by different manufacturers. Adapted from Uffmann M et al, Eur. J. Radiol. (2009).<sup>78</sup>

dose efficiency of the detector. Early stages of the concept were contributed by Albert Rose, who is known for the Rose Model of signal detectability that determines the visibility of an object depending on the object contrast relative to its background and the object size.<sup>82</sup> He was one of the founding fathers of the concept who realized that an ideal detector was limited only by quantum noise. In other words, the detector is only limited by random Poisson-distributed photons. It was when Rodney Shaw and Robert Wagner formulated the concept of the ideal observer performance for the different imaging modalities that the DQE was became used in the field of medical imaging.<sup>84;83;72</sup>

The ideal observer performance is related to the detectability index  $d'^2$  defined as<sup>81</sup>:

$$d'^2 = \int_{-\infty}^{\infty} \text{NEQ}(u) |\Delta S(u)|^2 du. \quad (1.2.1)$$

where  $\text{NEQ}(u)$  expresses image quality as the number of Poisson-distributed quanta

that would produce a given SNR given an ideal detector, and  $\Delta S(u)$  describes the frequency content of the object relative to a uniform background. The DQE can be determined by taking the ratio of NEQ to the average number of incident quanta per unit area  $\bar{q}$ , and the detectability index can then be written as:

$$d'^2 = \int_{-\infty}^{\infty} \bar{q} \text{DQE}(u) |\Delta S(u)|^2 du. \quad (1.2.2)$$

Equation 1.2.2 shows that increasing the DQE at frequencies of importance to  $\Delta S(u)$  will increase the detectability index which is related to the ability to see objects. Since then, many investigations have used the DQE as a fundamental metric to evaluate x-ray detector dose efficiency.<sup>38;87;65;66;68;48;22;45</sup> The International Electrotechnical Commission (IEC) 62220-1 document has been developed as the standard guide for investigators who wish to determine the DQE to ensure accurate results.<sup>91;90;89;88</sup> The DQE (Fig. 1.2.1) depends on the average number of incident quanta, detector gain, Modulation Transfer Function (MTF), and Wiener Noise Power Spectrum (NPS) given by<sup>19;21;18</sup>:

$$\text{DQE}(u) = \frac{\text{NEQ}(u)}{\bar{q}} = \frac{\bar{q} G^2 |\text{MTF}(u)|^2}{\text{NPS}(u)} \quad (1.2.3)$$

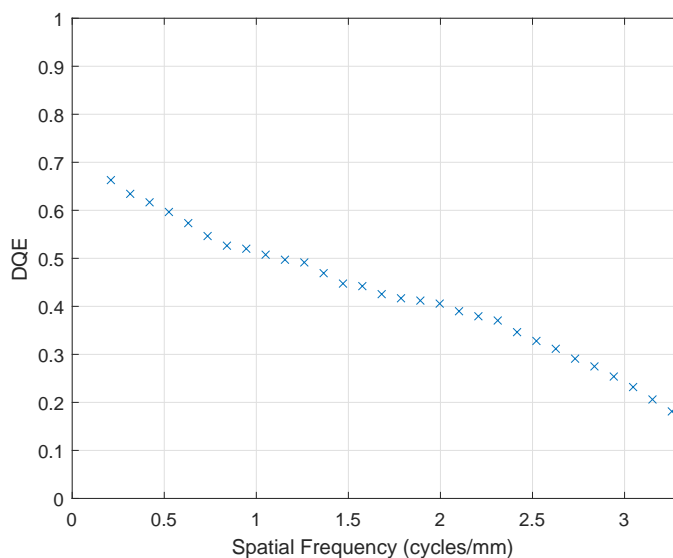


Figure 1.2.1: Illustration of the DQE of a digital detector

### 1.2.1 Linearization of Pixel Gain

The pixel gain ( $G$ ) is the slope of the detector system's characteristic response of a given x-ray detector. Since the DQE follows linear systems theory, the system characteristic response must be linear.<sup>31</sup> In other words, pixel gain must be the same across all exposures. If the pixel gain is not linear, the image must be linearized to ensure the DQE is properly calculated.<sup>88</sup> The IEC 62220-1 provides a guide for linearization that involves acquiring images using increasing and incrementally spaced exposures. This gives the system characteristic response across the exposures used by determining the relationship between air KERMA and pixel value. The conversion function is determined by evaluating the system characteristic response using the KERMA vs. pixel value graph (Fig. 1.2.2). The inverse of the conversion function is used for transformation of image data establishing a linear proportionality with respect to exposure.



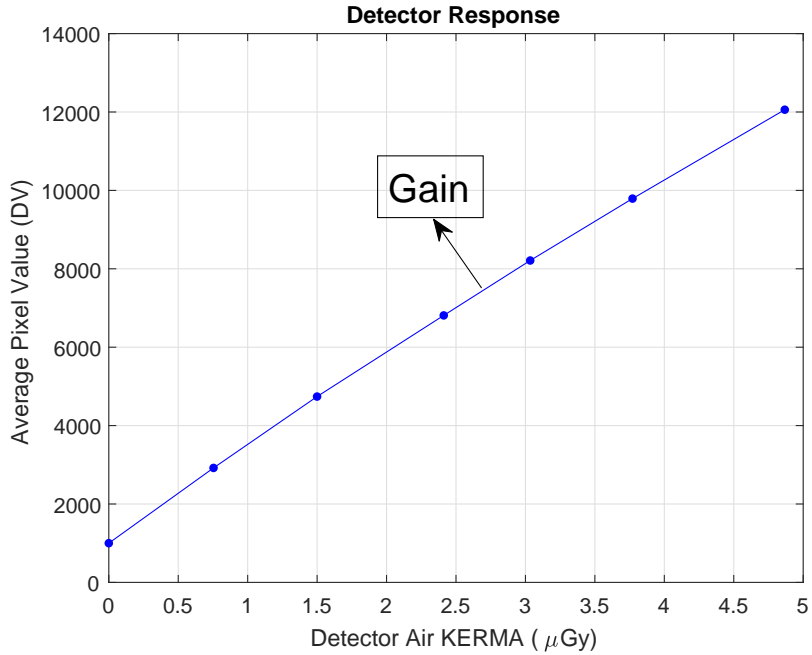


Figure 1.2.2: Illustration of a detector with slightly non-linear characteristic response

## 1.2.2 Modulation Transfer Function (MTF)

The MTF describes the spatial resolution of a x-ray detector. It is determined by measuring the response of a detector to an edge in the image. It can be measured using the wire, slit or slanted edge method.<sup>67;30;20</sup> The IEC 62220-1 document recommends use of the slanted edge method to determine the MTF (Fig. 1.2.3). Measuring the MTF involves first determining the oversampled edge spread function  $\text{ESF}(x)$  (Fig. 1.2.3). Differentiating  $\text{ESF}(x)$  gives the system line spread function  $\text{LSF}(x)$  (Fig. 1.2.3) that represents the detector impulse response to a line in one-direction given by:

$$\text{LSF}(x) = \frac{d}{dx}\text{ESF}(x). \quad (1.2.4)$$

Taking the Fourier Transform of  $\text{LSF}(x)$  gives the one-dimensional system optical transfer function  $\text{OTF}(u)$  defined as:

$$|\text{OTF}(u)| = \mathcal{F} \{ \text{LSF}(x) \} = \mathcal{F} \left\{ \frac{d}{dx} \text{ESF}(x) \right\} \quad (1.2.5)$$

The one-dimensional pre-sampling MTF is measured by taking the modulus of  $\text{OTF}(u)$  normalized to unity at zero-frequency given by:

$$\text{MTF}(u) = \frac{|\text{OTF}(u)|}{\text{OTF}(0)} \quad (1.2.6)$$

The MTF as a function of spatial frequency (Fig. 1.2.3) is a quantitative metric for spatial resolution that describes the ability of the detector system to preserve the contrast in an input signal.

### 1.2.3 Wiener Noise Power Spectrum

The distribution of x-ray quanta incident on an x-ray detector follows Poisson statistics.<sup>64;63;83;18</sup> In the context of an image, noise is related to the mean-square value of the fluctuation of a signal about its mean value or its variance.<sup>18</sup> One of the important realizations of Poisson statistics is that the mean number of x-ray quanta is equivalent to its variance. Therefore, image noise can be characterized by the variance of pixel values in the image. The autocovariance function measures image noise that describes whether random changes in the value of the function relative to the mean value correlate with changes from the mean at some distance.<sup>19;18</sup> The Wiener NPS  $W(u)$  (Fig. 1.2.4) is determined by taking the Fourier transform of the autocovariance function  $K_f$  according to the Wiener-Khinchin theorem given by:<sup>19;18</sup>

$$W(u) = \mathcal{F} \{ K_f(x) \} = \int K_f(x) e^{-2\pi i u x} dx. \quad (1.2.7)$$

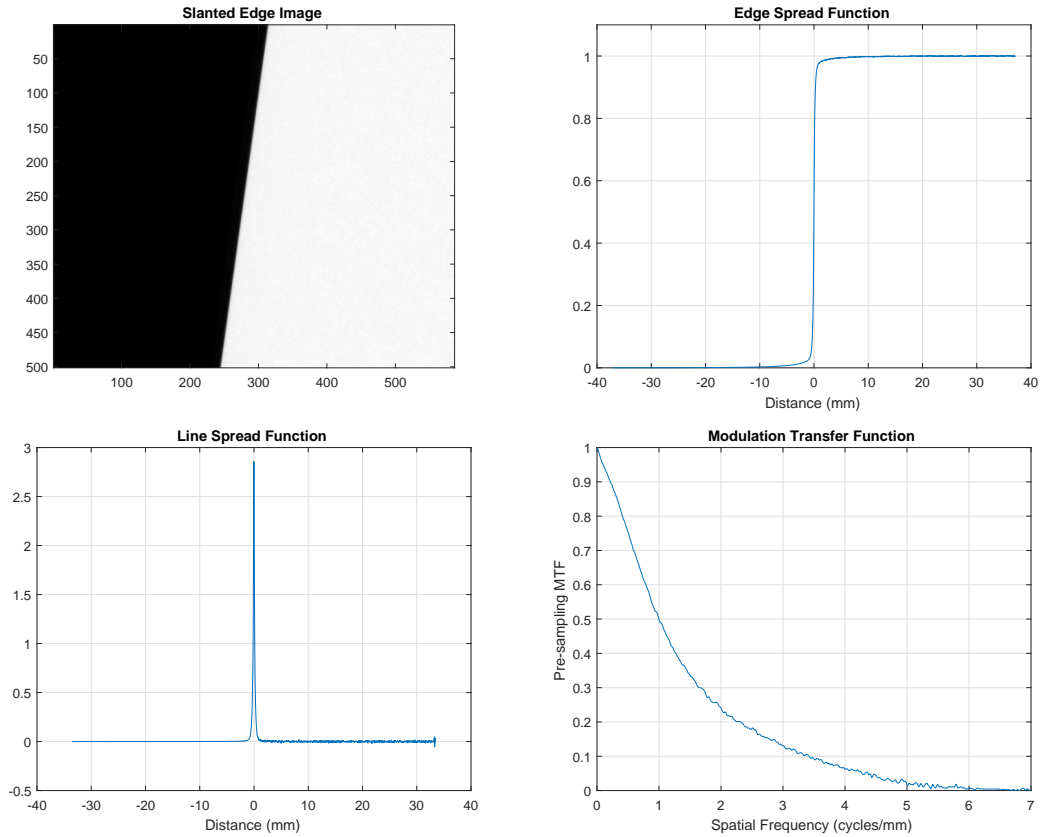


Figure 1.2.3: The edge spread function ESF (top right) is determined from the slanted edge image (top left). The MTF (bottom right) is calculated by differentiating the ESF and taking the Fourier Transform of the LSF (bottom left)

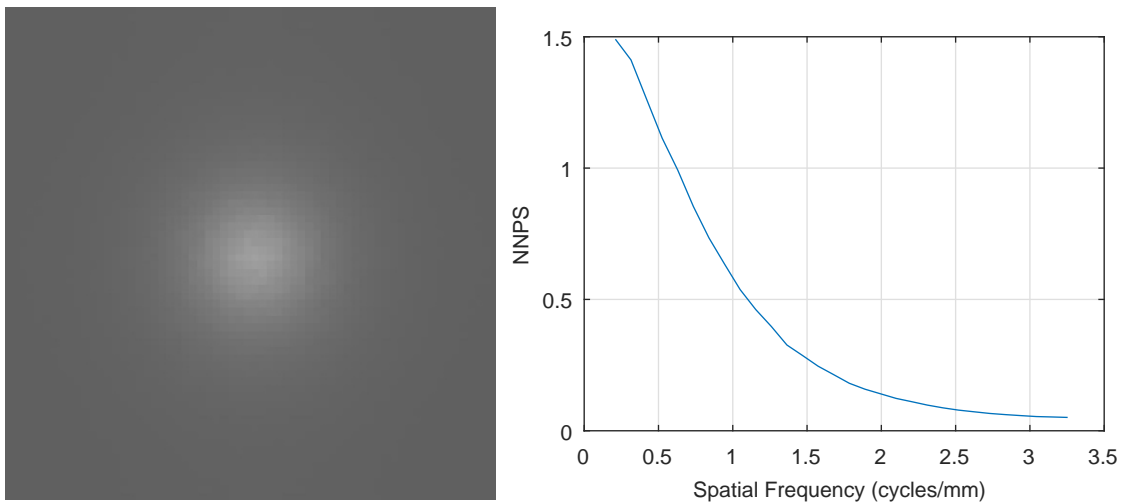


Figure 1.2.4: Illustration of the NPS in frequency space (left) and the one-dimensional normalized NPS (NNPS)(right)

### 1.3 Health Canada and Safety Code 35

Health Canada is responsible for helping Canadians maintain and improve their health, ensure that high-quality health services are accessible, and work to reduce health risks.<sup>2</sup> In the context of diagnostic x-ray imaging, the Safety Code 35 (SC35) document outlines safety procedures for installation, use and control of x-ray equipment in large medical radiological facilities. It outlines the responsibilities of personnel in minimizing radiation exposure to themselves and the patients, facility and equipment requirements, and quality assurance programs that ensures all clinical x-ray systems being used are performing optimally over the course of their lifetime.<sup>1</sup> These measures are in place to ensure patient exposures are kept as low as reasonably achievable (ALARA) without compromising the diagnostic quality of the x-ray image. All provincial and federal regulatory bodies including the Canadian Association of Medical Radiation Technologists (CAMRT), Healing Arts and Radiation Protection (HARP) Act, and the Safety Code 35 consider ALARA as a governing principle that is an integral part of the standard care of practice in medical imaging. This principle is further reinforced by multiple imaging campaigns like Image Wisely and Image Gently that aim to educate and remind clinical radiation workers of low dose x-ray imaging for all patients who need diagnostic x-ray imaging. It is widely understood that there is a delicate balance between image quality and exposure in diagnostic x-ray imaging. While many organizations at the federal and provincial level aim to regulate exposure, little to no attention is diverted to understanding how it may affect image quality (Fig. 1.3.1). The DQE as a function of spatial frequency, where low frequencies correspond with large objects and high spatial frequencies correspond with smaller fine-resolution objects, is a fundamental description of the ability of an x-ray detector to image different object sizes for a given exposure.



Figure 1.3.1: Illustration of the balance between image quality and exposure including the governing bodies that regulate exposure and the metrics currently used in clinics.

## 1.4 Using DQE in X-ray Imaging

Many investigators have used the DQE as a primary metric for evaluating detector performance.<sup>38;87;65;66;68;48;22;45</sup> It is particularly used for comparing different types of x-ray detector systems. For example, it has been shown that the DQE for flat panel DR systems are higher than CR systems.<sup>49;66;68;28</sup> It has been postulated that this is crucial for reduction of patient exposures without compromising image quality.<sup>10;38;77;5;79;44</sup> This is particularly important for longitudinal mammography breast cancer screening programs because use of higher performing DR systems can promote early breast cancer detection that is associated with improved patient prognosis.<sup>55;14;58;59;87;42</sup> The DQE clearly has vast implications starting from the research and manufacturer setting for improvement of x-ray detector dose efficiency, all the way to reducing patient exposures in the clinical environment.

Understanding the fundamental limitations of x-ray detectors in terms of their dose efficiency or DQE is lacking in the clinical environment. Unfortunately, a gap

persists in using the DQE in the clinical environment because of limited instrumentation and lack of expertise amongst clinical end users of x-ray systems. Therefore, end users do not have an evidence-based understanding of the fundamental efficiency limits of x-ray detectors, leaving patients vulnerable to being exposed to increased radiation exposures. With evidence showing that newly manufactured x-ray detectors ready for clinical use can vary by a factor of 2x to 10x in the DQE, patients are not receiving the same health benefits of high quality images for a given exposure.<sup>26</sup> Therefore, there is an existing need to measure the DQE in clinical environments to ensure patient safety.

## **1.5 DQE Measuring Device**

The Cunningham lab has developed an automated DQE-testing instrument called the DQEPro that is compliant with current IEC 62220-1 standards. It contains an ion chamber to determine an air KERMA measurement, two slanted-edge devices to measure the MTF in both x and y image dimensions, a 18 x 18 cm open-field area, and a fiducial marker frame to make an estimation of the relative distance from the image plane to the DQEPro to determine image plane exposure used for the DQE calculation. A software analysis tool that is integrated with the DQEPro is used to analyze the image data acquired for each DQE-analysis.

## **1.6 Research Objectives**

Our objective is to identify experimental burdens to the clinical end user when conducting a DQE analysis and ensure they are addressed to prevent DQE measurement errors in the clinical environment. This will be conducted using an automated and IEC-compliant method for measuring the DQE. Ultimately, this will provide clinical end-users with an evidence-based metric to monitor x-ray detector dose efficiency on

a longitudinal basis to ensure detectors are performing optimally for the acquisition of high quality images using low patient exposures.

## Bibliography

- [1] Health Canada. Safety code 35: Safety procedures for the installation, use and control of x-ray equipment in large medical radiological facilities. <https://www.canada.ca/en/health-canada/services/environmental-workplace-health/reports-publications/radiation/safety-code-35-safety-procedures-installation-use-control-equipment-large-medical-radiological-facilities-safety-code.html>. .
- [2] Health canada. <https://www.canada.ca/en/health-canada.html>.
- [3] Kasra Ahmadinia, J Benjamin Smucker, Clyde L Nash, and Heather A Vallier. Radiation exposure has increased in trauma patients over time. *Journal of Trauma and Acute Care Surgery*, 72(2):410–415, 2012.
- [4] Richard L. Morin Andrew D.A Maidment. Digital mammography: Coming of age. *American College of Radiology*, 2005.
- [5] Klaus Bacher, Peter Smeets, Kris Bonnarens, An De Hauwere, Koenraad Verstraete, and Hubert Thierens. Dose reduction in patients undergoing chest imaging: digital amorphous silicon flat-panel detector radiography versus conventional film-screen radiography and phosphor-based computed radiography. *American journal of roentgenology*, 181(4):923–929, 2003.
- [6] David J Brenner, Richard Doll, Dudley T Goodhead, Eric J Hall, Charles E Land, John B Little, Jay H Lubin, Dale L Preston, R Julian Preston, Jerome S Puskin, et al. Cancer risks attributable to low doses of ionizing radiation: assessing what we really know. *Proceedings of the National Academy of Sciences*, 100(24):13761–13766, 2003.

- [7] James A Brink. Dose tracking and rational examination selection for the medically-exposed population. *Health physics*, 106(2):225–228, 2014.
- [8] James A Brink and E Stephen Amis Jr. Image wisely: a campaign to increase awareness about adult radiation protection, 2010.
- [9] Helen C Burrell, D Mark Sibbering, AR Wilson, Sarah E Pinder, Andrew J Evans, Lindsey J Yeoman, Christopher W Elston, Ian O Ellis, Roger W Blamey, and JF Robertson. Screening interval breast cancers: mammographic features and prognosis factors. *Radiology*, 199(3):811–817, 1996.
- [10] HP Busch and K Faulkner. Image quality and dose management in digital radiography: a new paradigm for optimisation. *Radiation protection dosimetry*, 117(1-3):143–147, 2005.
- [11] ML Butler, L Rainford, J Last, and PC Brennan. Are exposure index values consistent in clinical practice? a multi-manufacturer investigation. *Radiation protection dosimetry*, 139(1-3):371–374, 2010.
- [12] Health Canada. X-ray equipment in medical diagnosis part a: Recommended safety procedures for installation and use - safety code 20a. .
- [13] Patricia A Carney, Diana L Miglioretti, Bonnie C Yankaskas, Karla Kerlikowske, Robert Rosenberg, Carolyn M Rutter, Berta M Geller, Linn A Abraham, Steven H Taplin, Mark Dignan, et al. Individual and combined effects of age, breast density, and hormone replacement therapy use on the accuracy of screening mammography. *Annals of internal medicine*, 138(3):168–175, 2003.
- [14] Anna M Chiarelli, Sarah A Edwards, Maegan V Prummel, Derek Muradali, Vicky Majpruz, Susan J Done, Patrick Brown, Rene S Shumak, and Martin J Yaffe. Digital compared with screen-film mammography: performance measures



- in concurrent cohorts within an organized breast screening program. *Radiology*, 268(3):684–693, 2013.
- [15] Mervyn D Cohen. Quality assurance: potential use for the newly described exposure index in clinical practice. *Journal of the American College of Radiology*, 7(10):748–749, 2010.
- [16] William David Coolidge. A powerful röntgen ray tube with a pure electron discharge. *Physical Review*, 2(6):409, 1913.
- [17] AR Cowen, AG Davies, and SM Kengyelics. Advances in computed radiography systems and their physical imaging characteristics. *Clinical radiology*, 62(12):1132–1141, 2007.
- [18] Ian A Cunningham. Applied linear-systems theory. *Handbook of medical imaging*, 1:121–122, 2000.
- [19] I. A. Cunningham and R. Shaw. Signal-to-noise optimization of medical imaging systems. *J. Opt. Soc. Am.*, 16(3):621–632, 1999.
- [20] IA Cunningham and BK Reid. Signal and noise in modulation transfer function determinations using the slit, wire, and edge techniques. *Medical physics*, 19(4):1037–1044, 1992.
- [21] J. C. Dainty and R. Shaw. *Image Science*. Academic Press, New York, 1974.
- [22] James T Dobbins, David L Ergun, Lois Rutz, Dean A Hinshaw, Hartwig Blume, and Dwayne C Clark. Dqe (f) of four generations of computed radiography acquisition devices. *Medical physics*, 22(10):1581–1593, 1995.
- [23] Steven Don, Marilyn J Goske, Susan John, Bruce Whiting, and Charles E Willis. Image gently pediatric digital radiography summit: executive summary. *Pediatric radiology*, 41(5):562–565, 2011.

- [24] Steven Don, Robert MacDougall, Keith Strauss, Quentin T Moore, Marilyn J Goske, Mervyn Cohen, Tracy Herrmann, Susan D John, Lauren Noble, Greg Morrison, et al. Image gently campaign back to basics initiative: ten steps to help manage radiation dose in pediatric digital radiography. *American Journal of Roentgenology*, 200(5):W431–W436, 2013.
- [25] Geoffrey G Eichholz. Managing patient dose in digital radiology, 2005.
- [26] Terenz R Escartin, Tomi F Nano, and Ian A Cunningham. Detective quantum efficiency: a standard test to ensure optimal detector performance and low patient exposures. In *SPIE Medical Imaging*, pages 97833W–97833W. International Society for Optics and Photonics, 2016.
- [27] AK Exadaktylos, Lorin Michael Benneker, V Jeger, L Martinolli, Harald Marcel Bonel, Stefan Egli, H Potgieter, and H Zimmermann. Total-body digital x-ray in trauma: an experience report on the first operational full body scanner in europe and its possible role in atls. *Injury*, 39(5):525–529, 2008.
- [28] Frank Fischbach, Jens Ricke, Torsten Freund, Michael Werk, Birgit Spors, Clemens Baumann, Maciej Pech, and Roland Felix. Flat panel digital radiography compared with storage phosphor computed radiography: assessment of dose versus image quality in phantom studies. *Investigative radiology*, 37(11):609–614, 2002.
- [29] US Preventive Services Task Force et al. Screening for breast cancer: Us preventive services task force recommendation statement. *Annals of internal medicine*, 151(10):716, 2009.
- [30] Hiroshi Fujita, D-Y Tsai, Takumi Itoh, Kunio Doi, Junji Morishita, Katsuhiko Ueda, and Akiyoshi Ohtsuka. A simple method for determining the modulation

- transfer function in digital radiography. *IEEE Transactions on medical imaging*, 11(1):34–39, 1992.
- [31] Jack D Gaskill. Linear systems, fourier transforms, and optics. *Linear Systems, Fourier Transforms, and Optics by Jack D. Gaskill New York, NY: John Wiley and Sons, 1978*, 1978.
- [32] Dale J Gibson and Robert A Davidson. Exposure creep in computed radiography: a longitudinal study. *Academic radiology*, 19(4):458–462, 2012.
- [33] Marilyn J Goske, Kimberly E Applegate, Coreen Bell, Jennifer Boylan, Dorothy Bulas, Penny Butler, Michael J Callahan, Brian D Coley, Shawn Farley, Donald P Frush, et al. Image gently: providing practical educational tools and advocacy to accelerate radiation protection for children worldwide. In *Seminars in Ultrasound, CT and MRI*, volume 31, pages 57–63. Elsevier, 2010.
- [34] Marilyn J Goske, Kimberly E Applegate, Jennifer Boylan, Priscilla F Butler, Michael J Callahan, Brian D Coley, Shawn Farley, Donald P Frush, Marta Hernanz-Schulman, Diego Jaramillo, et al. The image gently campaign: working together to change practice. *American Journal of Roentgenology*, 190(2):273–274, 2008.
- [35] Marilyn J Goske, Ellen Charkot, Tracy Herrmann, Susan D John, Thalia T Mills, Gregory Morrison, and Susan N Smith. Image gently: challenges for radiologic technologists when performing digital radiography in children. *Pediatric radiology*, 41(5):611, 2011.
- [36] Canadian Institute for Health Information. Medical imaging in canada 2007. 2007.
- [37] R Edward Hendrick. Radiation doses and cancer risks from breast imaging studies. *Radiology*, 257(1):246–253, 2010.

- [38] K Herrmann, H Bonel, A Stäbler, C Kulinna, C Glaser, N Holzknecht, B Geiger, M Schätzl, and M Reiser. Chest imaging with flat-panel detector at low and standard doses: comparison with storage phosphor technology in normal patients. *European radiology*, 12(2):385–390, 2002.
- [39] Phan T Huynh, Amanda M Jarolimek, and Susanne Daye. The false-negative mammogram. *Radiographics*, 18(5):1137–1154, 1998.
- [40] Karla Kerlikowske, Deborah Grady, John Barclay, Edward A Sickles, and Virginia Ernster. Effect of age, breast density, and family history on the sensitivity of first screening mammography. *Jama*, 276(1):33–38, 1996.
- [41] John M Lewin, R Edward Hendrick, Carl J DOrsi, Pamela K Isaacs, Lawrence J Moss, Andrew Karellas, Gale A Sisney, Christopher C Kuni, and Gary R Cutter. Comparison of full-field digital mammography with screen-film mammography for cancer detection: results of 4,945 paired examinations. *Radiology*, 218(3):873–880, 2001.
- [42] Seppo Lipasti, Ahti Anttila, and Martti Pamilo. Mammographic findings of women recalled for diagnostic work-up in digital versus screen-film mammography in a population-based screening program. *Acta Radiologica*, 51(5):491–497, 2010.
- [43] Nicholas W Marshall, Kim Lemmens, and Hilde Bosmans. Physical evaluation of a needle photostimulable phosphor based cr mammography system. *Medical physics*, 39(2):811–824, 2012.
- [44] N W Marshall, P Monnin, H Bosmans, F O Bochud, and F R Verdun. Image quality assessment in digital mammography: part i. technical characterization of the systems. *Physics in medicine and biology*, 56:4201–4220, July 2011. ISSN 1361-6560. doi: 10.1088/0031-9155/56/14/002.

- [45] Nicholas W. Marshall, Chantal van Ongeval, and Hilde Bosmans. Performance evaluation of a retrofit digital detector-based mammography system. *Physica Medica*, 32:312–22, Feb 2016.
- [46] Cynthia H McCollough, Beth A Schueler, Thomas D Atwell, Natalie N Braun, Dawn M Regner, Douglas L Brown, and Andrew J LeRoy. Radiation exposure and pregnancy: when should we be concerned? *Radiographics*, 27(4):909–917, 2007.
- [47] WE Muhogora, A Trianni, F Toso, A Devetti, R Padovani, P Msaki, and R Kazema. Comparison of image quality and patient dose for chest x-ray examinations on conventional and low cost computed radiography systems. *Radiography*, 18(4):275–278, 2012.
- [48] T. F. Nano, T. Escartin, E. Ismailova, K. S. Karim, J. Lindström, H. K. Kim, and I. A. Cunningham. MTF and DQE enhancement using an apodized-aperture x-ray detector design. *Med. Phys.*, 2017.
- [49] Ulrich Neitzel. Status and prospects of digital detector technology for cr and dr. *Radiation protection dosimetry*, 114(1-3):32–38, 2005.
- [50] Ulrich Neitzel. Management of pediatric radiation dose using philips digital radiography. *Pediatric radiology*, 34:S227–S233, 2004.
- [51] Noriaki Ohuchi, Koichi Yoshida, Michio Kimura, Akio Ouchi, Ken-ichi Shiiba, Koji Ohnuki, Akira Fukao, Rikiya Abe, Seiki Matsuno, and Shozo Mori. Comparison of false negative rates among breast cancer screening modalities with or without mammography: Miyagi trial. *Cancer Science*, 86(5):501–506, 1995.
- [52] Terue Okamura, Saori Tanaka, Koichi Koyama, Nishida Norihumi, Hideo Daikokuya, Toshiyuki Matsuoka, Kenji Kishimoto, Masakatsu Hatagawa, Hiroaki Kudoh, and Ryusaku Yamada. Clinical evaluation of digital radiography

- based on a large-area cesium iodide-amorphous silicon flat-panel detector compared with screen-film radiography for skeletal system and abdomen. *European radiology*, 12(7):1741–1747, 2002.
- [53] Sinead E Peters and Patrick C Brennan. Digital radiography: are the manufacturers’ settings too high? optimisation of the kodak digital radiography system with aid of the computed radiography dose index. *European radiology*, 12(9): 2381–2387, 2001. significantly lower than that recommended by manufacturers can be used of AP chest in mobile CR with no loss of image quality.
- [54] Etta D Pisano. Digital compared with screen-film mammography: Measures of diagnostic accuracy among women screened in the ontario breast screening program evidence that direct radiography is superior to computed radiography for cancer detection, 2016.
- [55] Etta D Pisano, Constantine Gatsonis, Edward Hendrick, Martin Yaffe, Janet K Baum, Suddhasatta Acharyya, Emily F Conant, Laurie L Fajardo, Lawrence Bassett, Carl D’orsi, et al. Diagnostic performance of digital versus film mammography for breast-cancer screening. *N Engl J Med*, 2005(353):1773–1783, 2005.
- [56] Etta D Pisano, Martin J Yaffe, Bradley M Hemminger, R Edward Hendrick, Loren T Niklason, Andrew DA Maidment, Carolyn M Kimme-Smith, Stephen A Feig, Edward A Sickles, and M Patricia Braeuning. Current status of full-field digital mammography. *Academic radiology*, 7(4):266–280, 2000.
- [57] Canadian Task Force on Preventive Health Care et al. Recommendations on screening for breast cancer in average-risk women aged 40–74 years. *Canadian Medical Association Journal*, 183(17):1991–2001, 2011.
- [58] Maegan V Prummel, Susan J Done, Derek Muradali, Vicky Majpruz, Patrick

- Brown, Hedy Jiang, Rene S Shumak, Martin J Yaffe, Claire MB Holloway, and Anna M Chiarelli. Digital compared to screen-film mammography: breast cancer prognostic features in an organized screening program. *Breast cancer research and treatment*, 147(2):389–399, 2014.
- [59] Maegan V Prummel, Derek Muradali, Rene Shumak, Vicky Majpruz, Patrick Brown, Hedy Jiang, Susan J Done, Martin J Yaffe, and Anna M Chiarelli. Digital compared with screen-film mammography: measures of diagnostic accuracy among women screened in the ontario breast screening program. *Radiology*, 278(2):365–373, 2015.
- [60] Wilhelm Conrad Röntgen. On a new kind of rays. *Science*, pages 227–231, 1896.
- [61] American College of Radiology et al. Image wisely, 2011.
- [62] Xiujiang J Rong, Chris C Shaw, Dennis A Johnston, Michael R Lemacks, Xinming Liu, Gary J Whitman, Mark J Dryden, Tanya W Stephens, Stephen K Thompson, Kerry T Krugh, et al. Microcalcification detectability for four mammographic detectors: Flat-panel, ccd, cr, and screen/film. *Medical physics*, 29(9):2052–2061, 2002.
- [63] Albert Rose. *Vision: human and electronic*. Springer Science & Business Media, 2013.
- [64] Albert Rose. The sensitivity performance of the human eye on an absolute scale. *JOSA*, 38(2):196–208, 1948.
- [65] Ehsan Samei and Michael J Flynn. An experimental comparison of detector performance for computed radiography systems. *Medical physics*, 29(4):447–459, 2002.

- [66] Ehsan Samei, Michael J Flynn, Harrell G Chotas, and James T Dobbins III. Dqe of direct and indirect digital radiography systems. In *Medical Imaging 2001*, pages 189–197. International Society for Optics and Photonics, 2001.
- [67] Ehsan Samei, Michael J Flynn, and David A Reimann. A method for measuring the presampled mtf of digital radiographic systems using an edge test device. *Medical physics*, 25(1):102–113, 1998.
- [68] Ehsan Samei, Simon Murphy, and Olav Christianson. DQE of wireless digital detectors: comparative performance with differing filtration schemes. *Med. Phys.*, 40:081910, August 2013. ISSN 2473-4209. doi: 10.1118/1.4813298.
- [69] CM Schaefer-Prokop, DW De Boo, M Uffmann, and M Prokop. Dr and cr: Recent advances in technology. *European journal of radiology*, 72(2):194–201, 2009.
- [70] J Anthony Seibert, David K Shelton, and Elizabeth H Moore. Computed radiography x-ray exposure trends. *Academic radiology*, 3(4):313–318, 1996.
- [71] R. Shaw. The equivalent quantum efficiency of the photographic process. *J Photogr Sc*, 11:199–204, 1963.
- [72] Rodney Shaw and Richard L VanMetter. An analysis of the fundamental limitations of screen-film systems for x-ray detection i. general theory. In *Application of Optical Instrumentation in Medicine XII*, pages 128–132. International Society for Optics and Photonics, 1984.
- [73] S Jeff Shepard, Jihong Wang, Michael Flynn, Eric Gingold, Lee Goldman, Kerry Krugh, David L Leong, Eugene Mah, Kent Ogden, Donald Peck, et al. An exposure indicator for digital radiography: Aapm task group 116 (executive summary). *Medical physics*, 36(7):2898–2914, 2009.



- [74] F Shtern. Digital mammography and related technologies: a perspective from the national cancer institute. *Radiology*, 183(3):629–630, 1992.
- [75] Malcolm Sperrin and John Winder. *X-ray imaging*. IOP Publishing, 2014.
- [76] Perry Sprawls. *Physical principles of medical imaging*. Aspen Publishers, 1987. [http://www.sprawls.org/ppmi2/FILMCON/The Characteristic Curve](http://www.sprawls.org/ppmi2/FILMCON/The%20Characteristic%20Curve).
- [77] Michael Strotzer, Markus Völk, Maximilian Reiser, Markus Lenhart, Christoph Manke, Josef Gmeinwieser, Nicolaus Holzknacht, Johann Link, and Stefan Feuerbach. Chest radiography with a large-area detector based on cesium-iodide/amorphous-silicon technology: Image quality and dose requirement in comparison with an asymmetric screen–film system. *Journal of thoracic imaging*, 15(3):157–161, 2000.
- [78] Martin Uffmann and Cornelia Schaefer-Prokop. Digital radiography: the balance between image quality and required radiation dose. *Eur J Radiol*, 72(2): 202–208, 2009.
- [79] Markus Völk, OkkaW Hamer, Stefan Feuerbach, and Michael Strotzer. Dose reduction in skeletal and chest radiography using a large-area flat-panel detector based on amorphous silicon and thallium-doped cesium iodide: technical background, basic image quality parameters, and review of the literature. *European radiology*, 14(5):827–834, 2004.
- [80] Eliseo Vano, José Miguel Fernández, José Ignacio Ten, Carlos Prieto, Luciano Gonzalez, Ricardo Rodriguez, and Hugo de Las Heras. Transition from screen-film to digital radiography: evolution of patient radiation doses at projection radiography. *Radiology*, 243(2):461–466, 2007.
- [81] W Vennart. Icru report 54 medical imaging - the assessment of image quality isbn 0-913394-53-x. april 1996, maryland, usa, 1997.

- [82] Robert F Wagner. Lessons from my dinners with the giants of modern image science. *Radiation protection dosimetry*, 114(1-3):4–10, 2005.
- [83] Robert F Wagner. Toward a unified view of radiological imaging systems. part ii: Noisy images. *Medical physics*, 4(4):279–296, 1977.
- [84] Robert F Wagner, Kenneth E Weaver, Earl W Denny, and Robert G Bostrom. Toward a unified view of radiological imaging systems. *Medical physics*, 1(1):11–24, 1974.
- [85] Charles E Willis. Computed radiography: a higher dose? *Pediatric radiology*, 32(10):745–750, 2002.
- [86] Image Wisely. Radiation safety in adult medical imaging. See <http://www.imagewisely.org/>(accessed March 28, 2011), 2013.
- [87] Martin J Yaffe, Aili K Bloomquist, David M Hunter, Gordon E Mawdsley, Anna M Chiarelli, Derek Muradali, and James G Mainprize. Comparative performance of modern digital mammography systems in a large breast screening program. *Medical physics*, 40(12), 2013.
- [88] Medical electrical equipment - characteristics of digital x-ray imaging devimag-ing Part 1-1: Determination of the detective quantum efficiency - Detectors used in radiographic imaging. Technical Report IEC 62220-1-1, International Electrotechnical Commission, 2015.
- [89] Medical electrical equipment - Characteristics of digital x-ray imaging devices - Part 1-3: Determination of the detective quantum efficiency - Detectors used in dynamic imaging. Technical Report IEC 62220-1-2, International Electrotechnical Commission, 2008.

- [90] Medical electrical equipment - Characteristics of digital x-ray imaging devices - Part 1-2: Determination of the detective quantum efficiency - Detectors used in mammography. Technical Report IEC 62220-1-2, International Electrotechnical Commission, 2007.
- [91] Medical electrical equipment - Characteristics of digital x-ray imaging devices - Part 1: Determination of the detective quantum efficiency. Technical Report IEC 62220-1, International Electrotechnical Commission, 2003.

## Chapter 2

### Detective Quantum Efficiency

### (DQE) Measurements in a Clinical Setting

## 2.1 Introduction

X-ray imaging is associated with a known small carcinogenic risk due to the use of ionizing radiation.<sup>27;7;3</sup> Since image quality in terms of signal-to-noise ratio (SNR) is related to the Poisson statistics of x-ray generation and detection, there exists a balance between high patient exposures to increase image quality and low exposures to reduce risks.

The ability of a detector to produce high SNR images for a given number of incident x-ray quanta is described by the detective quantum efficiency (DQE) which is the “equivalent” quantum efficiency<sup>35</sup> expressed as a function of spatial frequency  $u$ :<sup>13;11;12</sup>

$$\text{DQE}(u) = \frac{\text{NEQ}(u)}{\bar{q}} = \frac{\bar{q}G^2 |T(u)|^2}{W(u)} \quad (2.1.1)$$

$$= \frac{|T(u)|^2}{KQ_oW(u)/\bar{d}^2}, \quad (2.1.2)$$

where  $\bar{q}$  [ $\text{mm}^{-2}$ ] is the number of x-ray quanta per unit area incident on the detector in the image plane given by  $\bar{q} = KQ_o$ ,  $K$  [ $\mu\text{Gy}$ ] is the corresponding air KERMA,  $Q_o$  [ $\text{mm}^{-2}\mu\text{Gy}^{-1}$ ] is the number of x-ray quanta per unit area per unit KERMA associated with the spectrum,  $G$  is the slope of the curve relating detector signal as a linear digital value  $\bar{d}$  to  $\bar{q}$  given by  $G = d\bar{d}/d\bar{q}$ ,  $T(u)$  is the characteristic transfer function normalized to unity at  $u = 0$  with the modulation transfer function (MTF) given by  $|T(u)|$  and  $W(u)$  [ $\text{mm}^2$ ] is the image Wiener noise power spectrum (NPS). While this expression assumes a single x-ray energy, all quantities are measurable and it is widely accepted as a practical working definition.<sup>25</sup>

The DQE is widely used as a primary performance metric in detector research, manufacturing and evaluation, and is required by the US FDA for new device applications.<sup>1</sup> Despite much progress in detector development, many investigations<sup>31;20;33;39;10;37</sup> show there remains a wide variation in DQE across different x-ray systems, particu-

larly at high spatial frequencies, with the implication being that not all patients are benefiting from the same high-quality images for low exposures.

Average patient exposures are controlled by regulations in most jurisdictions, and initiatives are supported by a number of professional organizations to promote safe imaging practices such as the Image Gently Alliance.<sup>18;16;15</sup> In addition, manufacturers generally recommend quality assurance tests specific to their equipment to ensure selected specifications are maintained. However, the link between the two, that is achieving the best possible image quality for a given exposure, is not regulated and is surprisingly difficult to quantify and document. The DQE provides this information but DQE tests as described by IEC guidelines<sup>2;4;5;6;19;29</sup> are not well suited to clinical settings<sup>19</sup> and only a few leading facilities incorporate DQE testing into their quality assurance programs.<sup>19;21;22;23;24</sup> DQE information, if available, could be used effectively in a number of ways. For example, systems with the highest DQE might be preferred for pediatric imaging to minimize patient exposures. In addition, records of DQE results may help anticipate failing equipment and provide evidence-based decision making to maximize equipment lifetime and optimize replacement strategies.

Clinical end users operating x-ray systems are radiologic technologists who are often unfamiliar with the DQE-measurement process. Their prime responsibilities include ensuring patient safety and acquiring patient x-ray images, but are sometimes delegated to perform basic periodic testing on x-ray equipment. As a result, most end users have little understanding of the current state of their detector dose efficiency or DQE. This is compounded by the fact that low DQE performance can often be compensated for by increasing patient exposures, contributing to “dose creep”.<sup>38;14;17</sup>

DQE testing in a clinical setting provides specific challenges that make it difficult to achieve IEC compliance and ensure accurate results.<sup>19</sup> In this investigation, we examine some of these challenges and the effect they may have on DQE measurements, and describe the performance of an automated DQE-testing instrument evaluated in

a clinical setting.

## 2.2 Theory

With reference to Eq. (2.1.2), DQE results are dependent on the accuracy of several measured quantities, including:

1. Air KERMA  $K$  projected to the image plane, free of all scatter including back-scatter from the detector. This requires an accurate knowledge of the image plane position (may be concealed by a protective cover or in a wall or table Bucky), chamber-to-image distance (CID), and source-to-image distance (SID) to make an inverse-square correction to the image plane.
2. System MTF,  $|T(u)|$ , excluding any effects of focal-spot blur (some investigators include focal-spot blur in a measurement of the “effective” DQE<sup>8;34</sup>). This requires ensuring the MTF edge-test device is placed close to the image plane. If the edge is not sufficiently close for the source distance used, penumbral blur, off-focal radiation, and potentially scatter from the beam-hardening filter (eg. 21 mm Al for an RQA-5 spectrum) may affect results.
3. Image Wiener NPS,  $W(u)$ , normalized by the squared mean pixel value  $\bar{d}$  for linear and offset-corrected image data corresponding to  $K$ . Slight non-linearities in the system response can have a large effect on the DQE and hence linearity should always be validated and image data linearized when necessary.
4. The DQE requires use of a standard spectrum that has a specific nominal HVL as indicated by the IEC 62220-1 document. The recent (2015) IEC update has changed the nominal half-value layer (HVL) of the RQA-5 spectrum from 7.1 to 6.8 mm of Al. In addition, methods for attaining an RQA-5 spectrum have been changed from modifying the kV to changing the amount of added Al filtration to

achieve the standard HVL. Since the DQE depends on the quantum efficiency, it is possible the DQE can vary with different combinations of kV and added filtration while preserving the standard nominal HVL.

In this section we examine the challenges in determining each of these quantities in a clinical setting.

### 2.2.1 Air KERMA in Uncertain Image Plane

In a clinical setting it is generally impractical to remove the detector to measure air KERMA at the detector position, and it is necessary to place the chamber at a known position and implement an inverse-square correction. Air KERMA  $K$  projected to the image plane is given by

$$K = K_c \left( \frac{d_s - d_c}{d_s} \right)^2 = K_c \left( \frac{a_c}{a} \right)^2 \quad (2.2.1)$$

where  $K_c$  is the KERMA measured with an air chamber placed a distance  $d_c$  from the image plane and  $d_s$  is the source-image distance. In a clinical setting it may not be possible to know both  $d_s$  and  $d_c$  with sufficient accuracy. Our solution is to note that the inverse-square correction term can also be determined from the ratio  $a_c/a$  as shown in Eq. (2.2.1) where  $a_c$  and  $a$  are pixel spacings measured at the chamber and image planes respectively. Setting  $a$  to the known physical pixel spacing on the detector obtained from the DICOM header and measuring  $a_c$  with a frame containing fiducial markers constructed for the purpose and placed at the chamber position (Fig. 2.3.1) provides a method of determining the image-plane KERMA using Eq. (2.2.1) without requiring specific knowledge of  $d_s$  or  $d_c$ . The corresponding uncertainty variance is given by

$$\sigma_K^2 = \frac{a_c^4}{a^4} \sigma_{K_c}^2 + 2 \frac{a_c^2}{a^4} K_c \sigma_{a_c}^2. \quad (2.2.2)$$



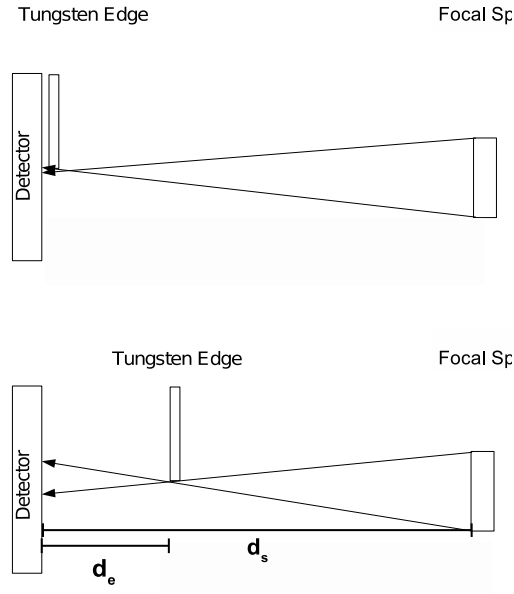


Figure 2.2.1: Illustration of focal-spot penumbral blur as the edge-image distance  $d_e$  is increased.

### 2.2.2 MTF with Increased Edge-plate Distance

The IEC recommends using the slanted-edge method which requires placing an edge-test device on the detector near the image plane.<sup>6;2;4;5</sup> An over-sampled edge profile is obtained from the slanted edge and differentiated to generate the line-spread function. The modulus of the Fourier transform is the MTF,  $|T(u)|$ .

Placing the edge close to the image plane can be a challenge in a clinical setting, particularly when using a wall or table bucky, often resulting in the edge plate positioned 5 to 7 cm from the image plane. Focal-spot penumbral blur may degrade results depending on the source-image distance, edge-image distance and focal spot size.

For a focal spot profile  $f(x')$  where  $x'$  indicates position on the source, penumbral blur on the image is described by  $f(x)$  where  $x = \frac{d_s - d_e}{d_e} x'$  [mm] indicates position in the image plane,  $d_e$  is the edge-image distance and  $d_s$  is the source-image distance

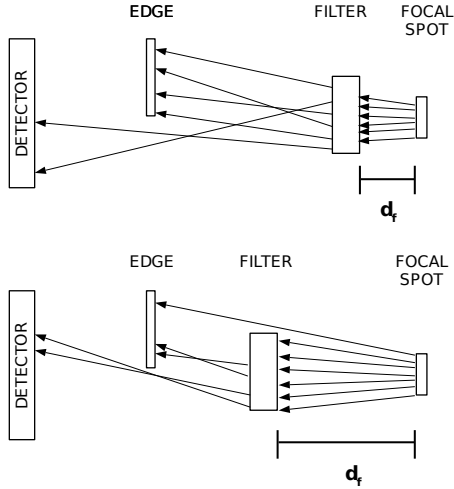


Figure 2.2.2: Illustration of blur caused by scatter from the beam-hardening filter as the filter distance  $d_f$  is increased.

required by IEC to be 150 cm or greater. The corresponding focal-spot transfer function is  $T_f(u)$  where:

$$T_f(u) = \frac{F(u)}{F(0)} \quad (2.2.3)$$

and  $F(u)$  is the Fourier transform of  $f(x)$ . The MTF measured with the slanted edge method is expected to scale with  $T_f(u)$  and since the NPS is measured from a uniform exposure, it is not affected by focal-spot blur and the DQE is expected to scale with  $T_f^2(u)$ .

Scatter generated in the beam-hardening filter (eg. 21 mm aluminum for an RQA-5 spectrum) may also be incident on the detector,<sup>9;30;36</sup> with an effect similar to off-focal radiation and not easily separated from focal-spot blur. The combined effect of filter scatter and focal spot blur is described by the product  $T_s(u)T_f(u)$  which can be measured experimentally using the method described by Nishiki.<sup>26</sup> With the edge placed close to the image plane the slanted edge method gives  $T(u)$ . With the edge placed far from the image plane it gives  $T_s(u)T_f(u)T(u)$ . The combined effect of focal

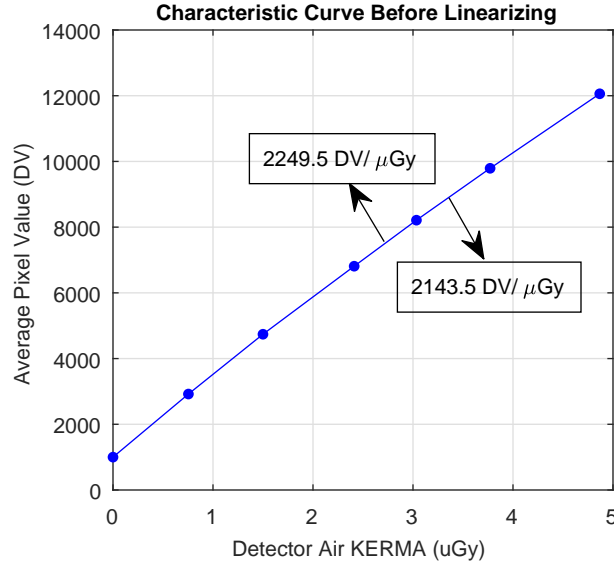


Figure 2.2.3: Illustration of the characteristic curve from a detector with a very slight non-linear response causing the slope of the characteristic curve to vary with detector KERMA. The nominal exposure used to measure the DQE was  $2.97 \mu\text{Gy}$ . System gain  $G$  is equal to the local slope at the nominal exposure.

spot blur and filter scatter,  $T_s(u)T_f(u)$ , is given by the ratio of the two:

$$T_s(u)T_f(u) = \frac{T_s(u)T_f(u)T(u)}{T(u)}. \quad (2.2.4)$$

The true DQE is a property of the detector in isolation, independent of focal-spot blur or filter scatter. However, the measured DQE is scaled by the square of  $T_s(u)T_f(u)$ .

### 2.2.3 Image Data Linearity

All Fourier metrics, including MTF and DQE, are valid only with linear image data such that pixel values are proportional to deposited x-ray energy (or detector air KERMA for a given spectral shape), corresponding to a constant slope of the characteristic curve. Non-linear transforms such as a logarithmic response, and even minor non-linearities such as illustrated in Fig. 2.2.3, must be assessed and linearized as required.

The DQE of a non-linear system can be determined using a small-signal approach , giving

$$\text{DQE}_{\Delta}(u) = \frac{\bar{q} \left| \frac{d\bar{d}}{d\bar{q}} \right|^2 |T(u)|^2}{W(u)} \quad (2.2.5)$$

and with reference to Eqs. (2.1.1) and (2.2.5), the relative error if not linearized is given by

$$\frac{\text{DQE}(u) - \text{DQE}_{\Delta}(u)}{\text{DQE}_{\Delta}(u)} = \frac{\left| \frac{\bar{d}}{\bar{q}} \right|^2 - \left| \frac{d\bar{d}}{d\bar{q}} \right|^2}{\left| \frac{d\bar{d}}{d\bar{q}} \right|^2} = \left| \frac{\bar{d}}{\bar{q}} \right|^2 \left| \frac{d\bar{d}}{d\bar{q}} \right|^{-2} - 1 \quad (2.2.6)$$

where  $\bar{d} = k\bar{q}A$  is the average dark subtracted pixel value, k is a constant of proportionality and A is the pixel area.

## 2.2.4 Beam Half Value Layer

The IEC Report 62220-1-1<sup>6</sup> outlines a standardized method for measuring the DQE for digital radiography to ensure accurate evaluation and comparison of x-ray detector performance. One of the items specified in the IEC protocol is the x-ray beam used to measure DQE. For example, the RQA-5 spectrum is defined by 70 kV tube voltage setting and 21 mm of aluminum (Al) filtration to achieve a half-value layer (HVL) of 6.8 mm of Al.<sup>28;29</sup> However, due to potential variations in x-ray tube output across different systems, the kV or Al thickness may have to be modified until the beam HVL (thickness producing 50% exposure transmission) matches the standard value of 6.8 mm. An earlier recommendation<sup>2</sup> of modifying the kV rather than Al thickness was more convenient. However, recent changes to the IEC document now recommends changing the Al thickness instead. In a clinical setting this process may be tedious and relatively slow. We investigated the DQE that results from different combinations of kV and Al thicknesses while sustaining the same HVL of 6.8 mm Al using a CsI digital detector. The quantum efficiency of a detector is given by

$$\alpha = \frac{\int_0^{E_m} \bar{q}(E)\alpha(E)E dE}{\int_0^{E_m} \bar{q}(E)E dE} \quad (2.2.7)$$

where

$$\alpha(E) = 1 - e^{-\left[\left(\frac{\mu}{\rho}\right)_{photo}(E) + \left(\frac{\mu}{\rho}\right)_{incoh}(E)\right]\rho l} \quad (2.2.8)$$

and  $\frac{\mu}{\rho}(E)$ ,  $\rho$  and  $l$  are the x-ray attenuation coefficient, density and thickness of the converter material respectively. For CsI, the fraction of photons absorbed is shown in (with  $\rho = 4.51 \text{ g/cm}^3$ ,  $l = 0.1 \text{ cm}$ ).

## 2.3 Materials and Methods

### 2.3.1 Detector Specifications

Our testing facility uses the Xmaru 1215CF-Master Plus CMOS flat panel detector (Xmaru, Rayence Co. Ltd., Seoul Korea). It is a CsI-based detector with an active area of 11.6 cm x 14.5 cm, physical element size of 49.5  $\mu\text{m}$ , and a 2352 x 2944 active matrix.

### 2.3.2 Image Plane Air KERMA

The ability to determine image-plane KERMA without knowing the image-plane position using Eq. (2.2.1) was validated using a plastic frame containing five fiducial markers on an 8.4x8.4 cm square (Fig. 2.3.1) placed in the chamber plane. The physical distance between markers divided by the average number of pixels between markers in each direction gives the pixel size in the chamber plane. To prevent back scatter radiation from contaminating the measured image plane exposure, the detector was removed and a reference ion chamber was positioned in its place that is 150 cm from the source. Five (5) exposure measurements were acquired and averaged using

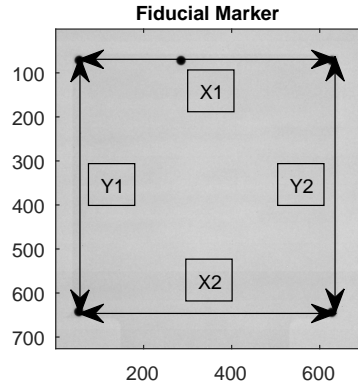


Figure 2.3.1: X-ray image of frame containing five fiducial markers on a  $8.4 \times 8.4$  cm square. Pixel spacing at the frame position is given by the number of pixels between markers divided by physical distance.

72 kV 50 mA 500 msec to determine an average image plane exposure ( $18.715 \mu\text{Gy}$ ). This was repeated at 2 cm, 4 cm, 6 cm, 8 cm, 10 cm and 20 cm from the image plane. Five (5) exposure readings were acquired and averaged at each position. Image plane exposures at each position were calculated using Eq. (2.2.1). The calculated image-plane exposures were compared to the measured image plane exposure determined by the reference ion chamber positioned at 150 cm.

### 2.3.3 Determining the Focal Spot Profile

The ratio of transfer functions Eq. (2.2.4) determined by the slanted-edge method was obtained by acquiring images of the 2 mm slanted tungsten edge device placed at  $d_e \approx 0$  and  $d'_e \approx 100$  cm relative to the image plane. Both edge images were dark-subtracted, linearized, open-field normalized and  $3 \times 3$  binned.

### Determining the MTF at Different Distances from the Image Plane

A 2-mm precision tungsten slanted edge positioned at distances 1.3 cm, 2.3 cm, 3.3 cm, 5.3 cm, 7.3 cm, 10.3 cm, and 21.3 cm from the image plane using a 150 cm and 100 cm

Source-to-Image Distance (SID). The slanted edge device was mounted and secured on a sliding stage that was manually moved incrementally at each distance. The distances from the image plane were measured with the side of the edge closest to the detector using a fixed tape measure on the stage. Two (2) open field images were acquired to determine an average open image. Two (2) slanted edge images were acquired at each distance and averaged. Both slanted edge and open field images were dark subtracted, 3x3 binned, and the average slanted edge images were open-field normalized. The MTF was determined by differentiating the oversampled edge spread function using the slanted edge method to obtain the system line spread function, and subsequently performing the Fourier Transform and normalizing by its zero-frequency value.<sup>32;6</sup>

## **Determining the MTF at Different Source Filter Distances (SFD)**

Here we position the RQA-5 filter at distances 16 cm, 20 cm, 30 cm, 50 cm and 70 cm from the focal spot using a 100 cm and 150 cm SID. The MTF was determined using the slanted edge device positioned at 1.3 cm and 10.3 cm from the image plane for each SFD. Images were dark subtracted, 3x3 binned, and the average slanted edge images were open-field normalized.

### **2.3.4 Linearization**

The DQE was analyzed using a RQA-5 spectrum [21 mm Al, 7.1 mm Al HVL]. Open-field images corresponding with air KERMA values of 0.7542, 1.500, 2.412, 3.034, 3.771 and 4.867  $\mu\text{Gy}$  were acquired. A plot of pixel value vs. air KERMA was generated to determine the system characteristic response. The inverse conversion function was determined from the system characteristic response and used to linearize

image data. Non-linearized and linearized image data were used to analyze the DQE.

### 2.3.5 Different Combinations of kV and Al Filtration

We validated our lab system's ability to produce an RQA-5 spectrum (IEC 62220-1-1 2015, 70 kV, 21 mm of Al, HVL = 6.8 mmAl) by measuring 50.4% attenuation at 6.47  $\mu$ Gy. A reference ion chamber was used to measure air KERMA 120 cm from the x-ray source. Fig. 2.3.3 shows the simulated x-ray spectra of the standard RQA-5 spectrum and the four beams with HVL 6.8mm: 65kV with 28 mm of Al, 67kV with 25mm of Al, 72kV with 18.8mm of Al and 76kV with 15.5mm of Al. Different kVs and filtrations that produce beams having the same HVL as a RQA-5 spectrum were also determined experimentally. The following combinations of kV and Al filtration were found to generate a x-ray beam having a HVL of 6.8mm of Al: 65kV with 28mm of Al, 67kV with 25mm of Al, 72kV with 18.8mm of Al, and 76kV with 15.5mm of Al producing 49.8%, 50.3%, 50.3% and 49.9% attenuation respectively (Fig. 2.3.2). These spectra were normalized to have the same total number of quanta. This was set to an equivalent air-kerma of 2.5 $\mu$ Gy exposure with an RQA-5 beam because that was the air-kerma used to measure DQE.

Figure 2.3.3 shows the simulated photon fluence absorbed in the CsI converter layer from the four different x-ray beams having the same HVL. In this simulation, we calculate the quantum efficiency of the 65kV+28mmAl, 67kV+25mmAl, 72kV+18.8mmAl and 76kV+15.5mmAl beams. The percent difference in their quantum efficiency relative to the IEC defined RQA-5 spectrum were 1.8%, 1.0%, -0.8%, and -2.2% respectively. We expect these beams to have different DQE(0) values with respect to an RQA-5 spectrum. We compared DQE measurements made by *DQEPro* (*DQEInstruments*, v. 4.6.1 and v. 5.0.0) using these x-ray beams. Images were dark subtracted and pixels were 3 x 3 binned. The DQE was measured at approximately the same nominal air KERMA of 2.62, 2.69, 3.23, 1.67, and 1.95 $\mu$ Gy for



65kV+28mmAl, 67kV+25mmAl, RQA5, 72kV+18.8mmAl, and 76kV+15.5mmAl x-ray beams respectively. Figure 2.3.2 is a plot of x-ray tube kV and amount of Al filtration required to produce a x-ray beam with a HVL of 6.8mm of Al. The solid line are simulated values using our lab package XRLib and the points are measured values. At 70kV, the amount of filtration (21mm of Al) matches perfectly with RQA5 as set by our packages. Filter predictions match well with measurements but could be less accurate as tube voltage is changed further from 70kV.

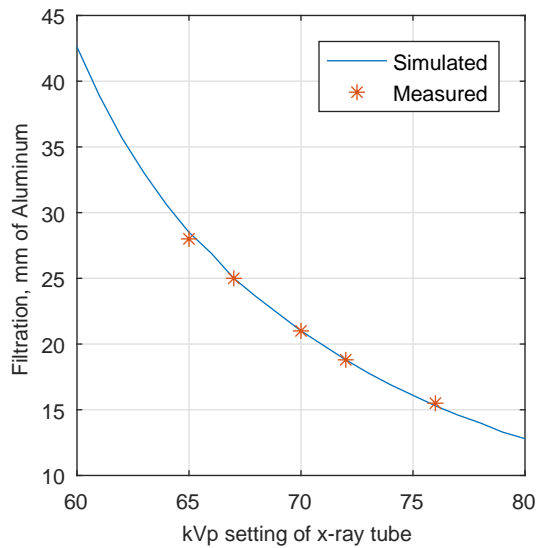


Figure 2.3.2: Aluminum filtration and tube kV settings for a x-ray beam HVL of 6.8mm of Al.

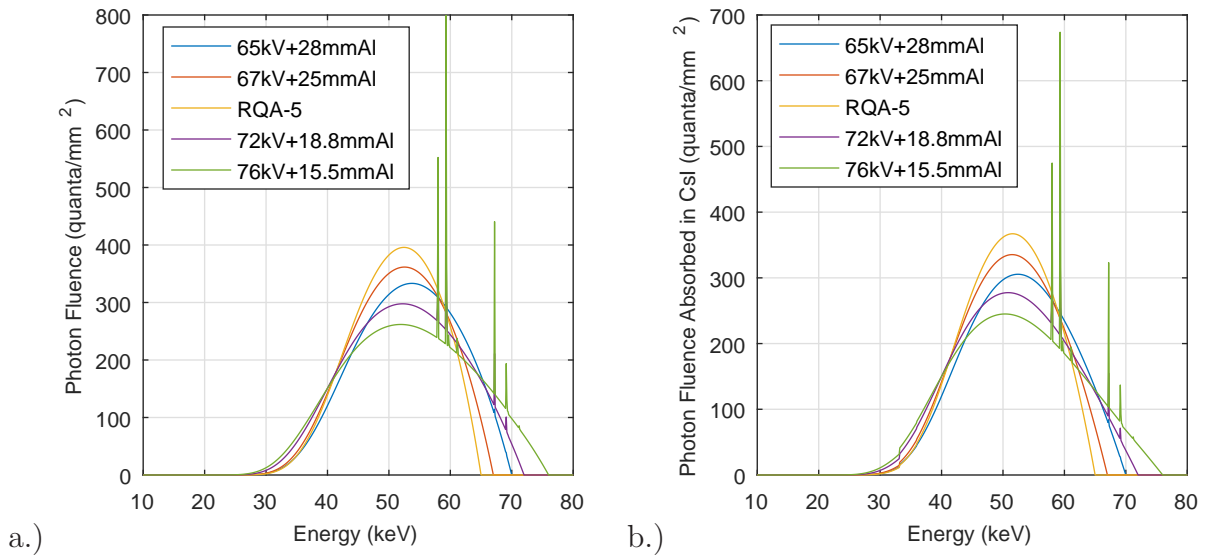


Figure 2.3.3: a.) Comparison of simulated x-ray beams using different combinations of kV and Al to generate a 6.8 mm Al HVL b.) Comparison of simulated photon fluence absorbed in CsI from three x-ray beams.

## 2.4 Results

### 2.4.1 Focal Spot Profile

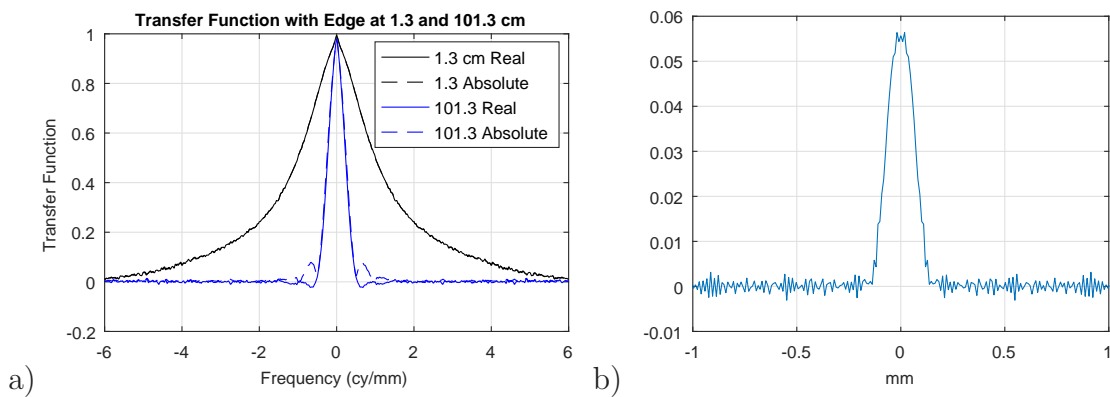


Figure 2.4.1: a) System transfer function obtained using the slanted-edge method with the edge placed at 1.3 cm and 101.3 cm from the image plane. b) Focal spot intensity profile as determined with Eq. 2.2.4

The focal spot profile was determined by taking the ratio of the transfer function calculated with the edge images acquired with the edge-device positioned at 101.3 cm

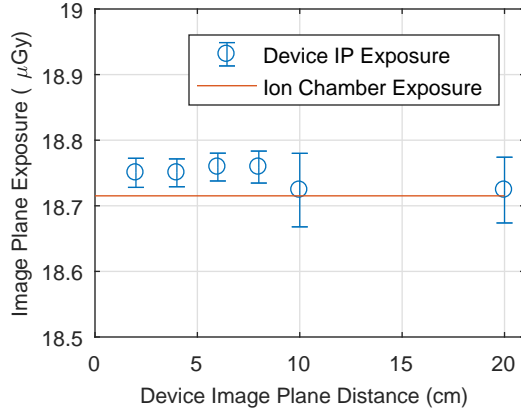


Figure 2.4.2: Plot of image-plane KERMA determined using Eq. (2.2.1) as a function of chamber distance from the image plane (SID = 150 cm). Error bars represent uncertainties  $\sigma_K$  determined by Eq. (2.2.2). The orange line shows the measured air KERMA using the ion chamber positioned at 150 cm

and 1.3 cm from the image plane (Fig. 2.4.1). The focal spot profile was determined to have a width of approximately 0.4 mm as shown in Fig. 2.4.1.

## 2.4.2 Image Plane Air KERMA Validation Using Fiducial Markers

Figure 2.4.2 shows measured air KERMA values as a function of device-to-image distance for a SID of 150 cm. Figure 2.4.2 shows consistent image plane exposure measurements calculated when the device is positioned up to 20 cm from the image plane. The calculated image plane air KERMA measurements for 2 cm, 4 cm, 6 cm, 8 cm, 10 cm and 20 cm were 18.750  $\mu Gy$ , 18.750  $\mu Gy$ , 18.759  $\mu Gy$ , 18.759  $\mu Gy$ , 18.724  $\mu Gy$ , 18.724  $\mu Gy$  [std = 0.022, 0.021, 0.021, 0.024, 0.056, 0.050] respectively.

## 2.4.3 Varying Distance of the MTF Edge from the Image Plane

Figure 2.4.3 shows the MTF degrading at higher frequencies as the edge distance is positioned farther away from the image plane. The degree of MTF degradation is

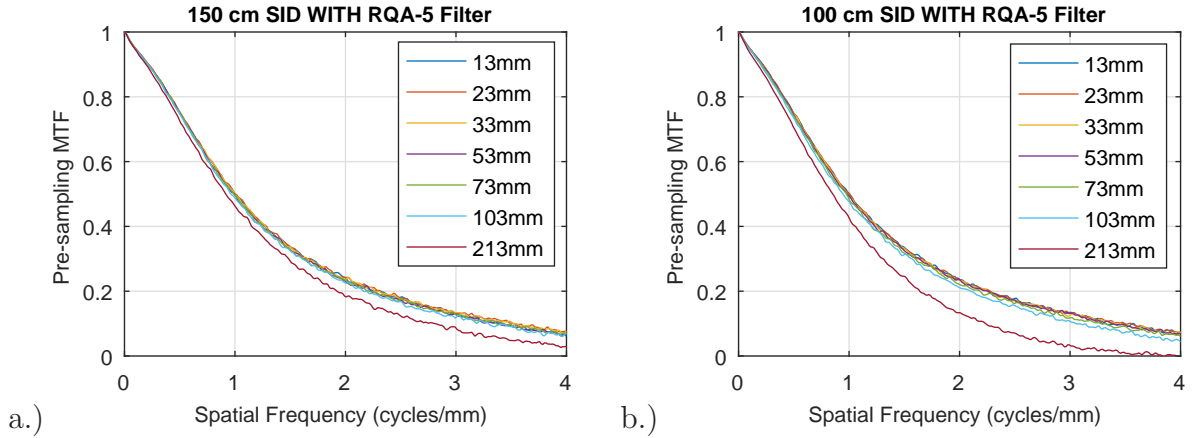


Figure 2.4.3: a.) MTF plot at different distances using a 150 cm SID, b.) MTF plot at different distances using a 100 cm SID

the same for distances up to 10.3 cm, while the MTF falls more drastically when the edge is placed at 21.3cm using a SID of 150 cm. The degradation of the MTF is more pronounced using a SID of 100 cm compared to a SID of 150 cm. The MTF starts degrading with the edge placed at 10.3 cm using a 100 cm SID because the effects of focal spot blurring increases as SID decreases. No observable differences is appreciated between edge placement distances of 1.3 cm and 7.3 cm using both 100 cm and 150 cm SID. The relative error across frequencies in the MTF with the edge placed at 2.3 cm, 3.3 cm, 5.3 cm, 7.3 cm were predominantly within 5%, with random fluctuations exceeding this error at higher frequencies when using an SID of 150 cm. The relative error in the MTF with the edge placed at 10.3 cm were within 5% at lower frequencies, while the relative error exceeded 5% at frequencies beyond 2 cycles/mm when using an SID of 150 cm. The relative error in the MTF with the edge positioned at 21.3 cm exceeded 5% predominantly across all spatial frequencies. Similar patterns were observed when using an SID of 100 cm.

## 2.4.4 Varying Distance of the Beam Hardening Filter from the Focal Spot

Figure 2.4.4 and Figure 2.4.5 show the MTF is preserved when the edge is positioned closest to the image plane (1.3 cm) while changing the distance of the RQA-filter relative to the focal spot. A low frequency drop in the MTF is observed when the edge is positioned at 10.3 cm from the image plane using an SID of 150 cm with the beam hardening Al filter positioned 70 cm from the focal spot (Fig 2.4.4b). Using a 100 cm SID shows a low frequency drop in the MTF when the beam hardening Al filter is positioned at 50 cm only when the edge is positioned 10.3 cm from the image plane (Fig 2.4.5d). A low frequency drop in the MTF is observed with the edge is positioned at 1.3 cm and 10.3 cm from the image plane when using a 100 cm SID and 70 cm SFD (Fig 2.4.5c and d).

### MTF Evaluated with a 150 cm SID

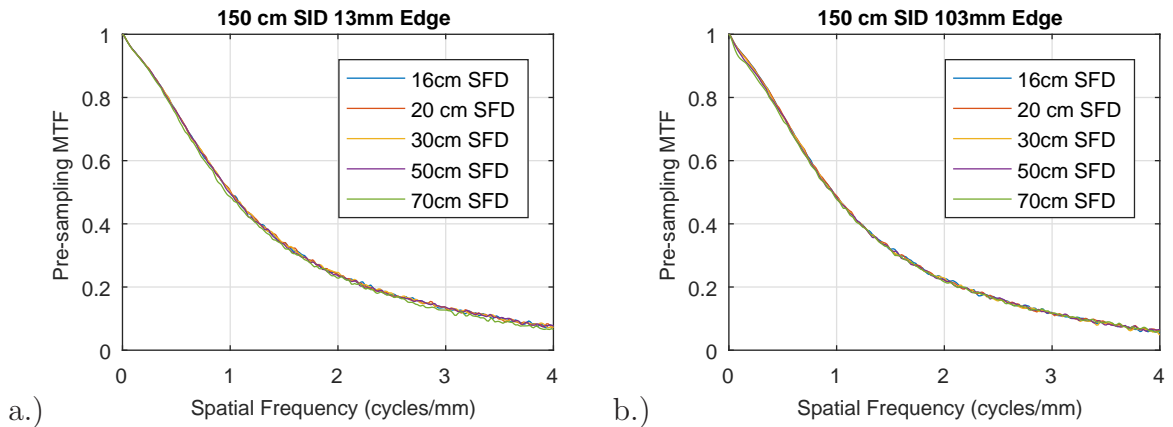


Figure 2.4.4: a.) MTF plot with the edge placed 13 mm from the image plane using a 150 cm SID while changing the SFD, b.) MTF plot with the edge placed at 103 mm from the image plane using a 150 cm SID.

## MTF Evaluated with a 100 cm SID

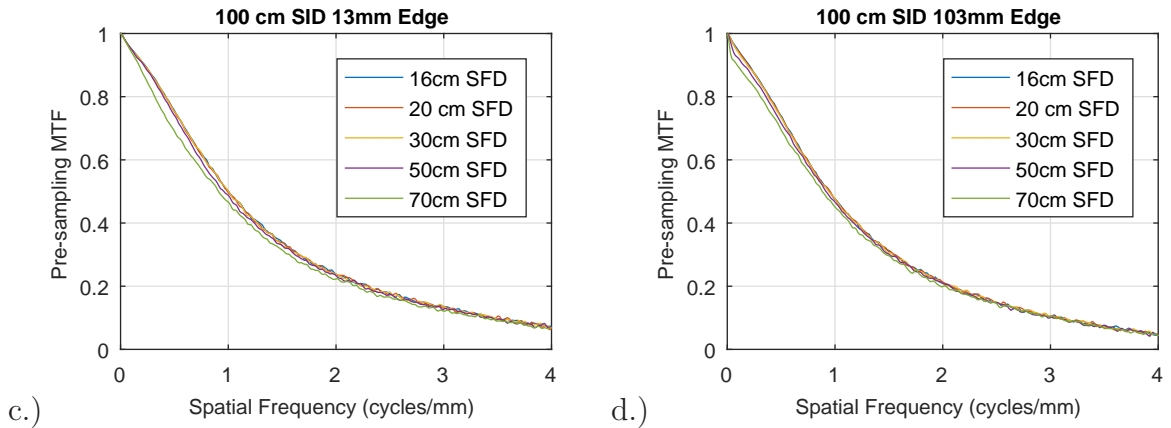


Figure 2.4.5: c.) MTF plot with edge placed at 13 mm from the image plane using a 100 cm SID, and d.) MTF plot with edge placed at 103 mm from the image plane using a 100 cm SID.

## 2.4.5 Different Combinations of kV and Al with the same HVL

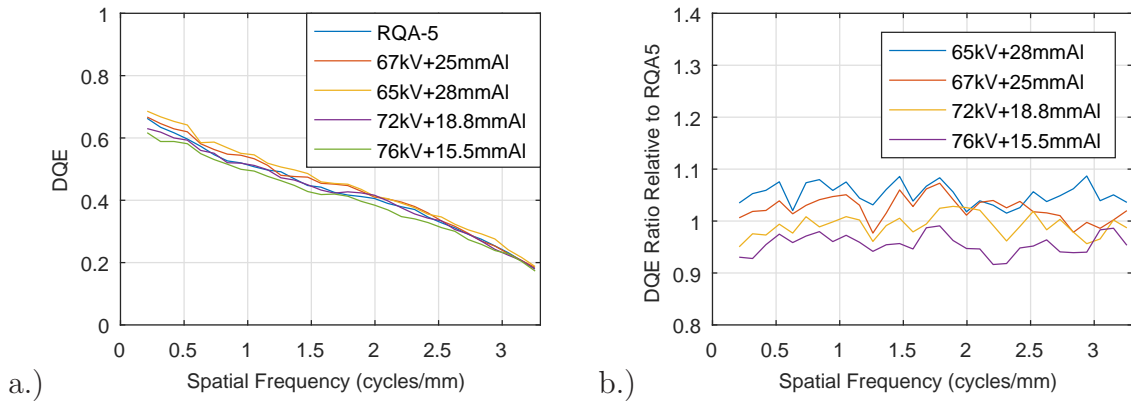


Figure 2.4.6: a.) Comparison of DQE curves acquired with different x-ray beams having the same HVL=6.8mm of Al but different kV and filtration. These DQEs were measured on the same detector with the same nominal air KERMA. b.) Ratio of DQE of the four spectra relative to the standard RQA-5 spectrum.

Figure 2.4.6a shows DQE curves for the five x-ray beams with 6.8 mm Al HVL. DQE at low frequencies for beams 65kV+28mmAl, 67kV+25mmAl, RQA5, 72kV+18.8mmAl,

and 76kV+15.5mm Al are 0.698, 0.696, 0.677, 0.646, and 0.628 corresponding to percent differences of +5.74%, +2.98%, -1.24%, -4.11% respectively. These results are similar and follow the same trend as theoretical predictions. We do not observe any frequency-dependent changes between different x-ray beams (Fig. 2.4.6b).

### 2.4.6 Linearized vs. Nonlinearized Image Data

There is an observed difference in the DQE due to non-linearity. The difference in the low frequency DQE appears greater between the nonlinearized and linearized image data compared to the high frequency DQE (Fig. 2.4.7). The average relative error in the DQE across all spatial frequencies between linearized and non-linearized image data is 17.1% [std = 1.06].

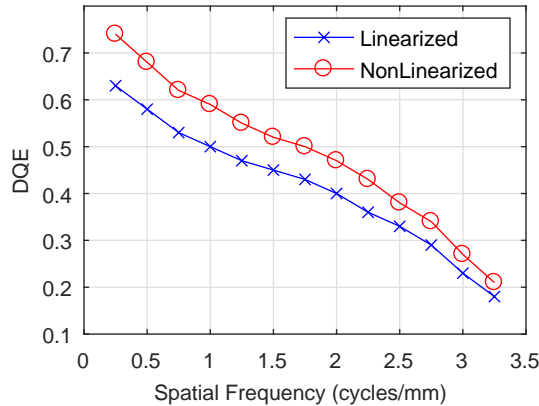


Figure 2.4.7: Comparison of DQE results using linearized vs. non-linearized image data.

## 2.5 Discussion

The calculated image plane air KERMA was determined within 2% accuracy by the device relative to the reference ion chamber. However, calculated image plane air KERMA with the device positioned at 10 cm and 20 cm from the image plane demonstrated greater standard deviation compared to measurements at 2 cm, 4 cm,

6 cm, and 8 cm. This observed greater standard deviation at 10 cm and 20 cm may be attributed to minor lateral offsets of the ion chamber due to geometric factors when moving the device closer to the source considering that the x-ray beam has a fixed collimation for our detector at a distance of 150 cm.

The calculated MTF was determined using clinically relevant SIDs of 100 cm and 150 cm. The edge positioned between distances 2.3 cm to 7.3 cm revealed stable MTF measurements relative to the MTF calculated at 1.3 cm with the relative error falling within 5%. A relative error exceeding 5% was observed with the edge placed at 10.3 cm from the image plane only at spatial frequencies beyond 2 cycles/mm. The degradation of the MTF was substantially observed with the edge positioned at 21.3 cm owing to the effects of focal spot penumbral blur.

Effects of scattered radiation from the beam modifying filter are most prominent when using a 100 cm SID and the edge plate positioned at 10.3 cm from the image plane. The MTF measurement is reproducible when the SFD is less than 30 cm using both 100 cm and 150 cm SID. Most, if not all, clinical x-ray systems will allow for positioning of the beam-modifying filter to be less than 30 cm SFD. Since the effects of scatter from the filter are more emphasized using a 100 cm SID, ensuring that the SFD is within 30 cm will be important for table bucky procedures because a SID of 150 cm is typically not achievable in this orientation.

Measurements of DQE using different x-ray beams with the same HVL as RQA-5 differed by as much as 5% across all spatial frequencies. An error in the DQE of this magnitude or more may result in a clinical setting if, 1) the beam kV is varied by 5keV or more, and 2) beam filtration is varied by 7mm of Al or more. These changes in beam settings to follow IEC defined HVL should be minimized and kept as close as possible to standard conditions for consistent DQE. Differences in DQE was observed to be independent of spatial frequency and indicates a different quantum efficiency measured for each beam. From Eqn. 2, DQE is calculated using



the number of x-ray quanta per unit area per unit KERMA [ $Q_o$ ], which depends on the x-ray beam parameters. Therefore, differences in  $Q_o$  values for different x-ray beams could account for measured DQE differences.

Linearization of image data is a fundamental requirement to ensure calculation of accurate DQE results. Figure 2.4.7 shows a substantial inflation of the DQE ( $\sim 17\%$ ) when images are not linearized. While this is specific to a detector response with a slightly non-linear characteristic response as shown in Figure 2.2.3, it is possible that detectors that have different characteristic responses will either over- or underestimate the detector DQE if not linearized correctly.

## 2.6 Conclusion

A comprehensive approach to identifying potential errors in measuring the DQE in the clinical environment is determined. These include:

- 1.) The image plane air KERMA was determined without exact knowledge of the position of the image plane. It is shown that the image plane air KERMA can be determined within 2% accuracy between distances 2 cm to 20 cm of the image plane. The robustness of this method ensures that the correct image plane air KERMA is measured independent of device-to-image plane distance.

- 2.) The MTF can be measured within 5% error using the slanted edge method within 10 cm of the image plane. It is recommended that the slanted edge device be positioned as close to the front face of the detector cover as possible. In the case where the edge device is  $\sim 10$  cm or more from the image plane, greater than 5% error in the MTF measurement at higher frequencies should be expected owing to the effects of focal spot blur. This is likely to appear when evaluating fixed table bucky detectors because of the increased distance between the image plane and the table surface compounded with limited SID. In this circumstance, we suggest using

the maximum allowable SID by the x-ray system, which typically falls somewhere between 100 cm and 150 cm depending on specific x-ray system set-up for a given x-ray room, to minimize penumbral blur contributions in the MTF measurement.

3.) Positioning of the RQA-5 filter relative to the focal spot does not affect the MTF unless the SFD is at least half the distance of the SID or greater (Fig. 2.4.4 and Fig. 2.4.5). Scatter contributions from the RQA-5 filter in the MTF measurement are most prominent with the edge device positioned 10.3 cm from the image plane. Since most clinical x-ray tubes allow for an SFD of less than 30 cm, the MTF can be measured with confidence despite variations in x-ray tube designs. In the circumstance where the SFD may be greater than 30 cm, the experimenter must ensure that the SFD is less than half the SID used to measure the DQE, and that the edge device be positioned as close to the image plane as possible.

4.) Use of kV settings  $\pm 3$  keV and Al filtration that is  $\pm 4$  mm relative to the standard RQA-5 spectrum is shown to not significantly affect the DQE measurement. The important criteria remains that the HVL must be at 6.8 mm of Al. We cannot make any conclusions whether modifying the kV or added Al filtration itself to achieve the standard x-ray beam HVL is more effective because we could not change either variable independently while sustaining the same HVL given the limitations of our x-ray tube kVp settings. It is important to note that there is flexibility in using different combinations of kV ( $\pm 5$  keV) and Al filtration ( $\pm 7$  mm) that may be necessary given variations in x-ray tube output across different x-ray systems without exceeding an error of 5% in the resulting DQE measurement.

5.) Linearizing the characteristic response of the detector is essential to achieve an accurate DQE measurement in clinical settings. While the relative error in the DQE using a detector with a slightly non-linear response overestimated the DQE by  $\sim 17\%$ , it is important to note that systems with different characteristic responses (i.e logarithmic transforms) may either under- or overestimate the DQE. Therefore,

access to the non-processed or raw image data sets should be made available by the manufacturer to the clinical user in order to ensure accurate and efficient DQE measurements.

In conclusion, this work gives light to the clinical end-user who may not be familiar with the DQE-measurement process to accurately measure the DQE of clinical x-ray detectors. This promotes use of the DQE as a primary metric for quality assurance and control practices in the clinical environment.

## 2.7 Acknowledgements

The authors are grateful for financial support from the Canadian Institutes of Health Research, and acknowledge the assistance of Michael McDonald, MEng, in constructing the x-ray system and device. We are grateful to Rayence Co. (Korea) for the high-performance CsI/CMOS detector and EMD Technologies (Canada) for the fast kV-switching generator.

- [1] Guidance for the submission of 510(k)'s for solid state x-ray imaging devices, 1999. Guidance for Industry and/or for FDA Reviewers/Staff and/or Compliance.
- [2] Medical electrical equipment - Characteristics of digital x-ray imaging devices - Part 1: Determination of the detective quantum efficiency. Technical Report IEC 62220-1, International Electrotechnical Commission, 2003.
- [3] Health risks from exposure to low levels of ionizing radiation: BEIR VII Phase 2. Technical report, National Research Council of the National Academies, 2006.
- [4] Medical electrical equipment - Characteristics of digital x-ray imaging devices - Part 1-2: Determination of the detective quantum efficiency - Detectors used in

- mammography. Technical Report IEC 62220-1-2, International Electrotechnical Commission, 2007.
- [5] Medical electrical equipment - Characteristics of digital x-ray imaging devices - Part 1-3: Determination of the detective quantum efficiency - Detectors used in dynamic imaging. Technical Report IEC 62220-1-2, International Electrotechnical Commission, 2008.
- [6] Medical electrical equipment - characteristics of digital x-ray imaging devimaging Part 1-1: Determination of the detective quantum efficiency - Detectors used in radiographic imaging. Technical Report IEC 62220-1-1, International Electrotechnical Commission, 2015.
- [7] Amy Berrington de González and Sarah Darby. Risk of cancer from diagnostic x-rays: estimates for the UK and 14 other countries. *Lancet*, 363(9406):345–351, 2004.
- [8] Marco Bertolini, Andrea Nitrosi, Stefano Rivetti, Nico Lanconelli, Pierpaolo Pattacini, Vladimiro Ginocchi, and Mauro Iori. A comparison of digital radiography systems in terms of effective detective quantum efficiency. *Medical physics*, 39(5):2617–2627, 2012.
- [9] Ann-Katherine Carton, Dirk Vandenbroucke, Luc Struye, Andrew DA Maidment, Yen-Hong Kao, Michael Albert, Hilde Bosmans, and Guy Marchal. Validation of mtf measurement for digital mammography quality control. *Medical Physics*, 32(6):1684–1695, 2005.
- [10] Anna M Chiarelli, Sarah A Edwards, Maegan V Prummel, Derek Muradali, Vicky Majpruz, Susan J Done, Patrick Brown, Rene S Shumak, and Martin J Yaffe. Digital compared with screen-film mammography: performance measures

- in concurrent cohorts within an organized breast screening program. *Radiology*, 268(3):684–693, 2013.
- [11] I. A. Cunningham and R. Shaw. Signal-to-noise optimization of medical imaging systems. *J. Opt. Soc. Am.*, 16(3):621–632, 1999.
- [12] Ian A Cunningham. Applied linear-systems theory. *Handbook of medical imaging*, 1:79–159, 2000.
- [13] J. C. Dainty and R. Shaw. *Image Science*. Academic Press, New York, 1974.
- [14] Steven Don. Radiosensitivity of children: potential for overexposure in cr and dr and magnitude of doses in ordinary radiographic examinations. *Pediatric radiology*, 34:S167–S172, 2004.
- [15] Steven Don, Marilyn J Goske, Susan John, Bruce Whiting, and Charles E Willis. Image gently pediatric digital radiography summit: executive summary. *Pediatr. Radiol.*, 41(5):562–565, 2011.
- [16] Steven Don, Robert MacDougall, Keith Strauss, Quentin T Moore, Marilyn J Goske, Mervyn Cohen, Tracy Herrmann, Susan D John, Lauren Noble, Greg Morrison, et al. Image gently campaign back to basics initiative: ten steps to help manage radiation dose in pediatric digital radiography. *Am. J. Roentgenol.*, 200(5):W431–W436, 2013.
- [17] Dale J Gibson and Robert A Davidson. Exposure creep in computed radiography: a longitudinal study. *Academic radiology*, 19(4):458–462, 2012.
- [18] Marilyn J Goske, Ellen Charkot, Tracy Herrmann, Susan D John, Thalia T Mills, Gregory Morrison, and Susan N Smith. Image gently: challenges for radiologic technologists when performing digital radiography in children. *Pediatr. Radiol.*, 41(5):611, 2011.

- [19] Hartmut Illers, Egbert Buhr, and Christoph Hoeschen. Measurement of the detective quantum efficiency (DQE) of digital X-ray detectors according to the novel standard IEC 62220-1. *Radiat. Prot. Dosim.*, 114(1-3):39–44, 2005.
- [20] Jonathan L Jesneck, Robert S Saunders, Ehsan Samei, Jessie Q Xia, and Joseph Y Lo. Detector evaluation of a prototype amorphous selenium-based full field digital mammography system. *Medical Imaging*, pages 478–485, 2005.
- [21] N W Marshall. Early experience in the use of quantitative image quality measurements for the quality assurance of full field digital mammography x-ray systems. *Physics in medicine and biology*, 52:5545–5568, September 2007.
- [22] N W Marshall, A Mackenzie, and I D Honey. Quality control measurements for digital x-ray detectors. *Physics in medicine and biology*, 56:979–999, February 2011.
- [23] Nicholas W. Marshall, Chantal van Ongeval, and Hilde Bosmans. Performance evaluation of a retrofit digital detector-based mammography system. *Physica Medica*, 32:312–22, Feb 2016.
- [24] K T Michael. The application of quantitative data analysis for the assessment of flat panel x-ray detectors in digital radiography as part of a quality assurance programme. *Biomedical Physics & Engineering Express*, 3(3):035004, 2017.
- [25] T. F. Nano, T. Escartin, E. Ismailova, K. S. Karim, J. Lindström, H. K. Kim, and I. A. Cunningham. MTF and DQE enhancement using an apodized-aperture x-ray detector design. *Med. Phys.*, 2017.
- [26] Masayuki Nishiki. Evaluation of the effective focal spot size of x-ray tubes by utilizing the edge response analysis. In *Proc. SPIE*, volume 9412, page 94123Z, 2015.

- [27] D A Pierce and D L Preston. Radiation-related cancer risks at low doses among atomic bomb survivors. *Radiation research*, 154:178–186, August 2000.
- [28] Nicole T Ranger, Ehsan Samei, James T Dobbins, and Carl E Ravin. Measurement of the detective quantum efficiency in digital detectors consistent with the iec 62220-1 standard: Practical considerations regarding the choice of filter material. *Medical physics*, 32(7):2305–2311, 2005.
- [29] Nicole T Ranger, Ehsan Samei, James T Dobbins III, and Carl E Ravin. Assessment of detective quantum efficiency: intercomparison of a recently introduced international standard with prior methods. *Radiology*, 243(3):785–795, 2007.
- [30] Frank Rogge, Hilde Bosmans, Peter Willems, and Guy Marchal. The use of mtf calculation in global and local resolution assessment in digital mammography. In *Proc. of SPIE Vol*, volume 5030, page 897, 2003.
- [31] Ehsan Samei and Michael J Flynn. An experimental comparison of detector performance for direct and indirect digital radiography systems. *Med. Phys.*, 30(4):608–622, 2003.
- [32] Ehsan Samei, Michael J Flynn, and David A Reimann. A method for measuring the presampled mtf of digital radiographic systems using an edge test device. *Medical physics*, 25(1):102–113, 1998.
- [33] Ehsan Samei, Simon Murphy, and Olav Christianson. DQE of wireless digital detectors: comparative performance with differing filtration schemes. *Med. Phys.*, 40:081910, August 2013.
- [34] Ehsan Samei, Nicole T Ranger, Alistair MacKenzie, Ian D Honey, James T Dobbins III, and Carl E Ravin. Detector or system? extending the concept of detective quantum efficiency to characterize the performance of digital radiographic imaging systems. *Radiology*, 249(3):926–937, 2008.

- [35] R. Shaw. The equivalent quantum efficiency of the photographic process. *J Photogr Sc*, 11:199–204, 1963.
- [36] SZ Shen, GE Mawdsley, AK Bloomquist, JG Mainprize, and MJ Yaffe. Interpreting system mtf and nps measured on clinical digital mammography systems. In *Digital Mammography*, pages 123–127. Springer, 2003.
- [37] N. Van Peteghem, H. Bosmans, and N. W. Marshall. NPWE model observer as a validated alternative for contrast detail analysis of digital detectors in general radiography. *Phys. Med. Biol.*, 61:N575–N591, Nov 2016.
- [38] Charles E Willis and Thomas L Slovis. The alara concept in pediatric cr and dr: dose reduction in pediatric radiographic exams—a white paper conference executive summary. *Pediatric radiology*, 34:S162–S164, 2004.
- [39] Martin J Yaffe, Aili K Bloomquist, David M Hunter, Gordon E Mawdsley, Anna M Chiarelli, Derek Muradali, and James G Mainprize. Comparative performance of modern digital mammography systems in a large breast screening program. *Medical physics*, 40(12), 2013.



## Chapter 3

# Conclusions and Future Directions

## 3.1 Overview and Research Questions

This thesis aims to address and reduce the experimental burden of measuring the DQE in the clinical environment. This is crucial because there continues to exist a wide variation in x-ray detector performance, and the DQE could be used for quality control and assurance purposes to ensure all patients are receiving the health benefits of high quality images while using low exposures.

## 3.2 Summary and Conclusions

We have shown that practical limitations in a clinical setting can affect DQE measurements. These include: 1) Determining the image plane exposure without knowing the image plane position; 2) Determining the MTF with the edge positioned at a substantial distance from the image plane due to the detector protective cover; 3) Determining the MTF with the spectrum-modifying filter positioned at a substantial distance from the source due to differences in x-ray tube cover designs; 4) Fine tuning the x-ray beam by changing aluminum and kV combinations while sustaining a 6.8mm Al HVL; and 5) Ensuring linear image data sets.

1.) We show that the image plane exposure can be determined by our fiducial marker method without having exact knowledge of the image plane location. This is particularly important in evaluating the DQE in the clinical setting because the image plane is often enclosed within a protective cover that varies across different manufacturers.

2.) The presence of the detector cover also affects the measurement of the MTF because it means the slanted-edge device cannot be positioned immediately adjacent to the image plane. We identified the limiting distance to which the slanted-edge device should be positioned before penumbral blur effects begin to degrade the MTF for two clinically relevant SIDs. This aims to notify the novice clinical end user to

ensure the relative distance between the DQE-measuring device to the image plane is appropriate.

3.) The inherent inability to position the edge immediately against the image plane in the clinical environment, compounded with the varying x-ray tube designs by different manufacturers may vary the SFD and contribute to inaccuracies of the MTF measurement because scatter radiation from the beam-modifying filter could be detected behind the slanted-edge device. We showed that the SFD must be less than at least one-half of the SID to measure the MTF without influence of scattered radiation from the beam modifying filter. Ultimately, this ensures that the end-user can measure the MTF accurately despite variations in x-ray tube protective cover designs across different systems.

4.) A standard RQA-5 spectrum with specifically defined combinations of kV and Al filtration that has a 6.8 mm Al HVL is mandated by the IEC to ensure accurate DQE measurements. Variations of x-ray tube outputs may require fine tuning of the kV parameters. However, recent changes to the IEC 62220-1 document stated that the amount of Al filtration be adjusted rather than the kV to fine tune the x-ray beam in order to achieve a 6.8 mm Al HVL. We showed that the DQE can be measured within 5% error given minimal changes to both the kV and Al filtration. This helps give confidence to clinical environments that may not have additional supplies of Al to follow the pre-defined standards of the IEC document in measuring the DQE using different kV and Al combinations. Despite the flexibility in using different combinations of kV and Al filtration without compromising the DQE measurement, sustaining an HVL of 6.8 mm Al remains to be the most important criteria for measuring the DQE using a RQA-5 spectrum, and that the IEC 62220-1 standard be followed accordingly.

5.) Linearization of images are fundamentally needed to ensure accurate DQE results. We showed that measuring the DQE without linearization of images could

inflate the DQE by close to 20%. These effects can mislead the clinical end user in postulating that their detector dose efficiency is significantly better than what it truly is. Consequently, patients may be receiving higher radiation exposures or low quality x-ray images.

We have identified the basic challenges that may arise when measuring the DQE in the clinical environment; and validated that the automated method can be used to alleviate experimental burden on the clinical end user. In summary, we have quantified these limitations and showed that acceptable results can be obtained with guidelines specified in Chapter 2.

### **3.3 Limitations**

While this work addressed limitations that currently exists in measuring the DQE in the clinical environment, there are other challenges that make it harder to promote use of the DQE for quality control and quality assurance purposes.

#### **3.3.1 Manufacturer Specific Image Processing**

Proprietary manufacturer specific image processing schemes alters the images acquired for a DQE analysis. Non-linear and adaptive image processing will cause the DQE measurement to fail using the current method. Access to unprocessed or raw image data is necessary for measuring the DQE because they are devoid of manufacturer specific non-linear image processing schemes. Despite the current state of the DQE-measurement process failing because of non-linear image processing, it has been suggested that a small signal method can potentially by-pass non-linear and adaptive processing while ensuring accurate DQE measurements.<sup>8</sup> This suggests that measuring the DQE of x-ray detector systems with non-linear or adaptive processing image data could be linearizable through the small signal approach to measure the

DQE.

### **3.3.2 Extraction of Images**

Some systems do not allow access of image data that are devoid of manufacturer specific processing unless a technical representative is present for routine maintenance of x-ray systems through QA mode. A way to by-pass this problem and gain access to the images is to export the images through PACS. However, it must be made sure that the images are merely not screen shots of the images acquired from the control station. Screen shots of images from the control station do not preserve the dynamic range of the images. These images are not indicative of the true detector system response. It is possible to coordinate with technical staff who monitor the PACS system to gain access to image data for a DQE analysis. While this may work well for large clinical settings who have dedicated technical support, smaller clinics may find this more inconvenient. Altogether, accessing images through PACS is a possibility but may be inconvenient for users who do not have direct access to their PACS system.

### **3.3.3 Length of Time for Analysis**

Performing routine maintenance on all x-ray systems is an integral part of ensuring patients are safe from overexposures. However, it is also crucial that all x-ray systems are available for use. Measuring the DQE accurately without having specific expertise or experience requires careful methodology to ensure accurate results. The automated device alleviates much of the experimental burden on the user by ensuring all moving parts and components are positioned adequately for the entire DQE measurement process. Clinical facilities will need to temporarily shut down an x-ray room to conduct an analysis, similar to current routine maintenance procedures. This can result in even longer wait times for patients who need x-ray imaging services, especially for

facilities with high patient throughput. While the DQE measurement process using the current automated method can be completed within 15 to 20 minutes for every detector, an updated version of an automated DQE-testing instrument is currently being developed to shorten this analysis time to approximately 5-10 minutes per detector system. We believe this will encourage widespread use of the DQE in clinical environments to ensure optimal detector performance without making x-ray rooms unavailable for a significant portion of time.

## 3.4 Future Directions

### 3.4.1 NEQ, DQE and the Exposure Index

Noise equivalent quanta (NEQ) expresses image quality on an absolute scale that is independent of specific system parameters given by<sup>6</sup>:

$$\text{NEQ}(\bar{q}, u) = \frac{|\bar{q}\mathbf{T}(u)|^2}{\text{NPS}(u)} \quad (3.4.1)$$

where  $\bar{q}$  is the average incident number of quanta,  $\mathbf{T}(u)$  is the system transfer function and  $\text{NPS}(u)$  is the noise power spectrum that quantified image noise. It gives the number of Poisson-distributed quanta that would produce the same SNR given an ideal detector. An image with a greater NEQ corresponds to lower image noise.<sup>6</sup> It is related to the DQE by:

$$\text{DQE}(u) = \frac{\text{NEQ}(u)}{\bar{q}} \quad (3.4.2)$$

The exposure index is currently being used as a standard for determining the optimal exposures used for specific x-ray imaging procedures as a way to indirectly

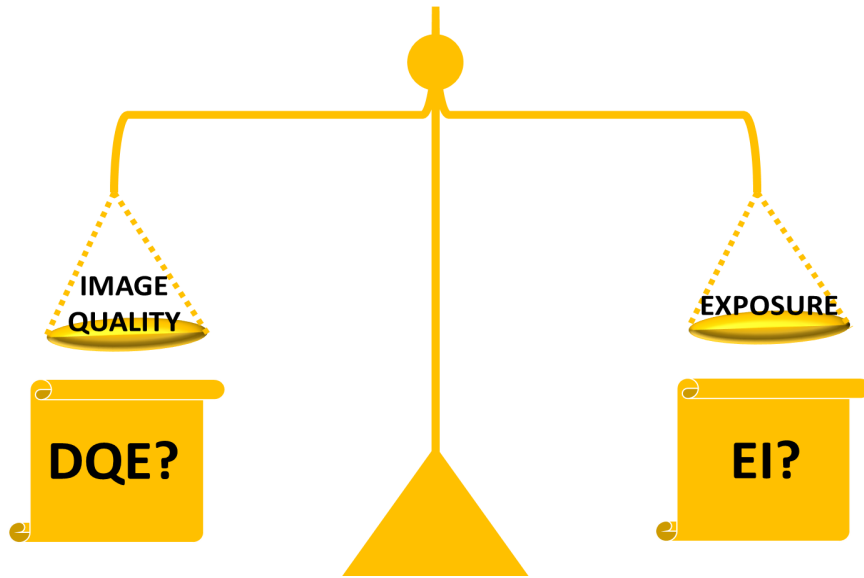


Figure 3.4.1: Illustration of DQE as a potential standardized metric used in combination with NEQ and EI to quantitatively sustain the balance between image quality and exposure

determine patient exposures.<sup>4;11;5;10</sup> However, a current limitation to using the EI effectively in clinical environments exists because manufacturers define it differently.<sup>13</sup> Since the DQE is a fundamental metric that characterizes the dose efficiency of all x-ray detectors, relating the DQE with the EI to establish a new standard indicator that would be grounded by fundamental principles accounting for both image quality and exposure has the potential to more effectively describe x-ray detector performance. It will also provide clinical end users a more comprehensive understanding of how modifications of exposures affect image quality. In principle, the DQE could complete this proper safeguarding of ensuring high quality images for low patient exposures (Fig. 3.4.1).

### 3.4.2 DQE and Technique Charts

Identifying the fundamental limitations of x-ray detectors will help distinguish their capabilities in performing specific x-ray procedures. The DQE can be used as a quantitative tool to strategically optimize technical factors used in clinical environments.

Many investigations are already studying the possibility of reducing exposures for specific radiographic procedures that include chest radiography, skeletal studies, and mammography because the medical imaging community is realizing the superiority of CR and DR systems in their dose efficiency without sacrificing the diagnostic quality of images.<sup>2;7;12;9</sup> Furthermore, the DQE can be used to dedicate x-ray detector systems for radiographic-specific procedures. For example, patients requiring fine resolution imaging for the purposes of identifying microcalcifications or chest nodules should be taken in a radiographic suite with a detector that has high DQE. Patients who do not require fine resolution imaging like scoliosis studies or orthopedic follow-up exams can use systems that may not have high enough DQE, but still provides the health benefits of the procedure. This will allow for testing of systems under the same conditions they are used on a frequent basis.

### **3.4.3 Cloud-Based Analysis of DQE**

Currently, the DQE analysis is conducted immediately after the acquisition of images for every x-ray detector evaluated. Opportunities for implementing remote analysis of the DQE could help centralization of monitoring centre-specific x-ray detector performance. This will help with careful maintenance and on-going tracking of x-ray system performance across all clinical centres.

### **3.4.4 DQE Survey of Digital Detectors**

The Ministry of Health and Long Term Care provides x-ray inspection services. Medical x-ray facilities will need to gain approval from The Ministry of Health and Long Term Care prior to being able to use an x-ray system. Establishing a survey of digital x-ray detectors could help x-ray inspection processes for expediting approval of new x-ray systems, replacement and/or upgrade of older models by establishing a centralized catalogue of x-ray detector performance in terms of the DQE. This provides



the inspector additional information to make a more well-informed decision of the dose efficiency of digital x-ray detectors. Furthermore, this can be used as a way to determine how the DQE degrades over time. It gives a way of ensuring x-ray systems are not used if they are deteriorating or cannot serve their purpose by providing diagnostic quality images without exposing the patient to higher radiation exposures.

### **3.5 Implications of Research**

Providing the instrumentation to measure the DQE clinically allows facilities to have a quantitative and evidence-based metric to determine the dose efficiency of their detectors. Immediate benefits of the instrument include providing evidence-based quality assurance practices that ensures on-going optimal detector performance, pioneering of the first DQE-survey to determine the current state of x-ray digital detectors in south-western Ontario, and improved awareness of the DQE and its implications among clinicians and technologists. The ultimate goal of a quality assurance program is to ensure accurate and timely diagnosis and treatment while minimizing dose deposited to both the patient and staff.<sup>1</sup> In Canada, quality assurance guidelines for x-ray imaging systems and facilities are primarily governed by Health Canada through the Safety Code 35.<sup>3</sup> This federal document outlines x-ray equipment and facility requirements that are needed to be fulfilled before being cleared for clinical use. Section C Chapter 2.1 Table 10 in the SC35 document outlines the criteria to be assessed for image receptor performance evaluations. It includes dynamic range, contrast detectability, modulation transfer function, noise and many others. While there certainly is not an explicit description of the DQE in this federal document, all factors contributing to this performance metric already exists. Therefore, all that is needed is to provide the means to combine all mandated criteria needed to determine the DQE. This is provided by our DQE-testing instrument. Further improvements to the

instrument will allow for a cloud-based approach to archive a library of DQE-results of all participating facilities who use digital x-ray detectors. This will help identify the current state of x-ray digital detectors in south-western Ontario, and will serve as the first initiative to promote widespread adoption of using the DQE in clinics to identify x-ray detector performance across Canada.

- [1] Health Canada. <https://www.canada.ca/en/health-canada.html>.
- [2] Klaus Bacher, Peter Smeets, Kris Bonnarens, An De Hauwere, Koenraad Verstraete, and Hubert Thierens. Dose reduction in patients undergoing chest imaging: digital amorphous silicon flat-panel detector radiography versus conventional film-screen radiography and phosphor-based computed radiography. *American journal of roentgenology*, 181(4):923–929, 2003.
- [3] Health Canada. Safety code 35: Safety procedures for the installation, use and control of x-ray equipment in large medical radiological facilities. <https://www.canada.ca/en/health-canada/services/environmental-workplace-health/reports-publications/radiation/safety-code-35-safety-procedures-installation-use-control-equipment-large-medical-radiological-facilities-safety-code.html>.
- [4] Mervyn D Cohen. Quality assurance: potential use for the newly described exposure index in clinical practice. *Journal of the American College of Radiology*, 7(10):748–749, 2010.
- [5] International Electrotechnical Commission et al. Medical electrical equipment—exposure index of digital x-ray imaging systems-part 1: Definitions and requirements for general radiography. *IEC, Geneva, Switzerland*, pages 62494–1, 2008.
- [6] Ian A Cunningham. Applied linear-systems theory. *Handbook of medical imaging*, 1:121–122, 2000.

- [7] K Herrmann, H Bonel, A Stäbler, C Kulinna, C Glaser, N Holzknecht, B Geiger, M Schätzl, and M Reiser. Chest imaging with flat-panel detector at low and standard doses: comparison with storage phosphor technology in normal patients. *European radiology*, 12(2):385–390, 2002.
- [8] Michael C McDonald. A method to measure the detective quantum efficiency of radiographic systems in clinical setting. 2012.
- [9] Etta D Pisano. Digital compared with screen-film mammography: Measures of diagnostic accuracy among women screened in the ontario breast screening program evidence that direct radiography is superior to computed radiography for cancer detection, 2016.
- [10] J Anthony Seibert and Richard L Morin. The standardized exposure index for digital radiography: an opportunity for optimization of radiation dose to the pediatric population. *Pediatric radiology*, 41(5):573, 2011. Standardized EI: Figure of different EI defined When actual EI and Target EI are equal, then DI is = 0.
- [11] S Jeff Shepard, Jihong Wang, Michael Flynn, Eric Gingold, Lee Goldman, Kerry Krugh, David L Leong, Eugene Mah, Kent Ogden, Donald Peck, et al. An exposure indicator for digital radiography: Aapm task group 116 (executive summary). *Medical physics*, 36(7):2898–2914, 2009.
- [12] Michael Strotzer, Markus Völk, Maximilian Reiser, Markus Lenhart, Christoph Manke, Josef Gmeinwieser, Nicolaus Holzknecht, Johann Link, and Stefan Feuerbach. Chest radiography with a large-area detector based on cesium-iodide/amorphous-silicon technology: Image quality and dose requirement in comparison with an asymmetric screen–film system. *Journal of thoracic imaging*, 15(3):157–161, 2000.

- [13] Martin Uffmann and Cornelia Schaefer-Prokop. Digital radiography: the balance between image quality and required radiation dose. *European journal of radiology*, 72(2):202–208, 2009.

# Appendix A

## Copyright Permissions for Figures Used in Chapter 1

**ELSEVIER LICENSE  
TERMS AND CONDITIONS**

Jul 24, 2017

---

This Agreement between Robarts Research Institute -- Terenz Escartin ("You") and Elsevier ("Elsevier") consists of your license details and the terms and conditions provided by Elsevier and Copyright Clearance Center.

License Number	4155480193619
License date	Jul 24, 2017
Licensed Content Publisher	Elsevier
Licensed Content Publication	Academic Radiology
Licensed Content Title	Exposure Creep in Computed Radiography A Longitudinal Study
Licensed Content Author	Dale J. Gibson,Robert A. Davidson
Licensed Content Date	Apr 1, 2012
Licensed Content Volume	19
Licensed Content Issue	4
Licensed Content Pages	5
Start Page	458
End Page	462
Type of Use	reuse in a thesis/dissertation
Portion	figures/tables/illustrations
Number of figures/tables/illustrations	1
Format	electronic
Are you the author of this Elsevier article?	No
Will you be translating?	No
Original figure numbers	Figure 1. Plot of intensive and critical care unit chest x-ray indicating optimal, over-,and underexposed exposure indexes percentages between August 2007 and December 2009
Title of your thesis/dissertation	Determining the Detective Quantum Efficiency (DQE) of X-ray Detectors in Clinical Environments
Expected completion date	Aug 2017
Estimated size (number of pages)	70
Requestor Location	Robarts Research Institute 1151 Richmond Street  London, ON N6A5B7 Canada Attn: Robarts Research Institute
Total	0.00 CAD
Terms and Conditions	

Dear Terenz Randolph Escartin,

Thank you for your request to reproduce IOP Publishing material in your thesis.

We are happy to grant permission for the use you request on the terms set out below.

**Details**

Title of ebook: Scientific Basis of the Royal College of Radiologists Fellowship

ebook author(s): Malcolm Sperring and John Winder

Citation/DOI: <https://doi.org/10.1088/978-0-7503-1058-1>

Copyright owner: IOP Publishing Ltd.

Figure number: 2.23

For use only in: Thesis

Permission granted to: Terenz Randolph Escartin

**Conditions**

Non-exclusive, non-transferrable, revocable, worldwide, permission to use the material in electronic form will be granted **subject to the following conditions:**

- Permission will be cancelled without notice if you fail to fulfil any of the conditions of this letter.
- You will reproduce the following prominently alongside the material:
  - the source of the material, including author, ebook title, and date of first publication. This information can be contained in a footnote or reference note; or
  - a link back to the ebook abstract (via DOI); and
  - the words "© IOP Publishing. Reproduced with permission. All rights reserved"
- The material will not, without the express permission of the author(s), be used in any way which, in the opinion of IOP Publishing, could distort or alter the author(s)' original intention(s) and meaning, be prejudicial to the honour or reputation of the author(s) and/or imply endorsement by the author(s) and/or IOP Publishing.
- Payment of £0 is received in full by IOP Publishing prior to use.

**Special Conditions – For STM Signatories ONLY (as agreed as part of the STM Guidelines)**

Any permissions granted for a particular edition will apply also to subsequent editions and for editions in other languages, provided such editions are for the work as a whole in situ and does not involve the separate exploitation of the permitted illustrations or excerpts.

**ELSEVIER LICENSE  
TERMS AND CONDITIONS**

Jul 24, 2017

This Agreement between Robarts Research Institute -- Terenz Escartin ("You") and Elsevier ("Elsevier") consists of your license details and the terms and conditions provided by Elsevier and Copyright Clearance Center.

License Number	4155480699283
License date	Jul 24, 2017
Licensed Content Publisher	Elsevier
Licensed Content Publication	European Journal of Radiology
Licensed Content Title	Digital radiography: The balance between image quality and required radiation dose
Licensed Content Author	Martin Uffmann,Cornelia Schaefer-Prokop
Licensed Content Date	Nov 1, 2009
Licensed Content Volume	72
Licensed Content Issue	2
Licensed Content Pages	7
Start Page	202
End Page	208
Type of Use	reuse in a thesis/dissertation
Intended publisher of new work	other
Portion	figures/tables/illustrations
Number of figures/tables/illustrations	1
Format	electronic
Are you the author of this Elsevier article?	No
Will you be translating?	No
Original figure numbers	Fig. 3. List of terms for exposure indices for various digital systems and their relationship to traditional dose measure (in Gy). In the second column, the proposal for an international standardisation is detailed (courtesy of Ulrich Neitzel, Philips Med
Title of your thesis/dissertation	Determining the Detective Quantum Efficiency (DQE) of X-ray Detectors in Clinical Environments
Expected completion date	Aug 2017
Estimated size (number of pages)	70
Requestor Location	Robarts Research Institute 1151 Richmond Street  London, ON N6A5B7 Canada Attn: Robarts Research Institute



# Curriculum Vitae

Name: Terenz Escartin

Year of birth: 1993

## Education and Training

09/15-present M.Sc Candidate

Department of Medical Biophysics

University of Western Ontario

London, Ontario, Canada

**Thesis:** Determining The Detective Quantum Efficiency (DQE) Of  
X-ray Detectors in Clinical Environments

**Supervisor:** Dr. Ian Cunningham

09/12-05/15 B.Sc. (Hon.) Honors Specialization in Medical Radiation Sciences

University of Toronto - St. George

Toronto, Ontario, Canada

09/12-05/15 Advanced Diploma - Radiological Technology

The Michener Institute for Applied Health Sciences

Toronto, Ontario, Canada

## Academic Awards, Scholarships, and Distinctions

- 09/15-09/17 Western Graduate Research Scholarship  
\$1500 per year for 2 consecutive years
- 09/16-05/17 Proteus Innovation Competition - Champions (**\$7500**)  
Western University - Synaptive Medical & World Discoveries
- 06/2017 London Imaging Discovery Day Poster Competition - 1st place (**\$300**)  
Western University - Schulich School of Medicine & Dentistry

## Publications

Nano, Tomi F., **Terenz Escartin**, Elina Ismailova, Karim S. Karim, Jan Lindstrom, Ho Kyung Kim, and Ian A. Cunningham. "MTF and DQE Enhancement using an Apodized-Aperture X-Ray Detector Design." *Medical Physics* (2017).

**Escartin, Terenz R.**, Tomi F. Nano, and Ian A. Cunningham. "Detective quantum efficiency: a standard test to ensure optimal detector performance and low patient exposures." In *SPIE Medical Imaging*, pp. 97833W-97833W. International Society for Optics and Photonics, 2016.

Nano, Tomi, **Terenz Escartin**, Karim S. Karim, and Ian A. Cunningham. "A novel x-ray detector design with higher DQE and reduced aliasing: Theoretical analysis of x-ray reabsorption in detector converter material." In *SPIE Medical Imaging*, pp. 978318-978318. International Society for Optics and Photonics, 2016.